1
2
3
4
5
6
7
8
9
10
11
12
13
14 **Mechanisms of physical-biological-biogeochemical interaction at the oceanic mesoscale**
15
16 Dennis J. McGillicuddy, Jr.
17
18 Department of Applied Ocean Physics and Engineering
19 Woods Hole Oceanographic Institution
20 Woods Hole, MA 02543, USA.
21 Email: dmcgillicuddy@whoi.edu
22
23
24
25 March 31, 2015
26

27
28 Table of Contents
29

55
56

57   **Abstract**
58
59   Mesoscale phenomena are ubiquitous and highly energetic features of ocean circulation.
60   Their influence on biological and biogeochemical processes varies widely, stemming from not
61   only advective transport but also through generation of environmental variations that affect
62   biological and chemical rates. Elucidation of the attendant mechanisms of physical-biological-
63   biogeochemical interaction is made difficult by the ephemeral nature of the underlying
64   processes, necessitating the use of multidisciplinary approaches involving *in situ* observations,
65   remote sensing, and modeling. All three aspects are woven through this review in an attempt to
66   synthesize current understanding of the topic, with particular emphasis on novel developments in
67   recent years.
68
69
70
71
72
73   **Key words**
74
75   Eddies, eddy pumping, advection, eddy-wind interaction, eddy-driven stratification, plankton
76   diversity.
77
78
79

1. INTRODUCTION

Interconnection among the physics, biology, and biogeochemistry of the sea stems from three basic sources. First, the rates of biological and chemical reactions depend on environmental parameters such as temperature, salinity, nutrient concentration, etc. Second, hydrodynamic transport continually redistributes dissolved and suspended constituents in the water column. Third, constituents of interest can have directed motion through the water as a result of buoyancy (sinking or floating) and behavior (swimming) in the case of motile organisms. Each of these three aspects supports a variety of mechanisms creating biological and biogeochemical variability at a wide range of space and time scales. For example, the difference in deep water nutrient concentrations between the North Atlantic and North Pacific basins has been attributed to the joint effects of the global overturning circulation and remineralization of sinking particulate material (Broecker & Peng 1982).

A particularly strong manifestation of physical-biological-biogeochemical interactions takes place at the oceanic mesoscale. The currents, fronts, and eddies that comprise this class of phenomena occur on spatial scales of tens to hundreds of kilometers, and are in many ways dynamically analogous to atmospheric weather. Mesoscale motions are typically produced by instability processes that result in flow features that are in approximate geostrophic balance in the horizontal and hydrostatic balance in the vertical; they are characterized by small Rossby and Froude numbers, as well as small aspect ratios. Of course the mesoscale occurs within a continuum of scales, bounded above by the large scale that sets the mean gradients from which eddies are generated, and bounded below by the submesoscale, in which motions are also significantly influenced by rotation and stratification but ageostrophic effects play a primary role in the balance of forces. Although the dynamics of mesoscale eddies and fronts are closely related, we will focus here mostly on the former. For a recent review on the nature and consequences of oceanic eddies from a primarily physical point of view, see McWilliams (2008).

Targeted studies of the biological impacts of mesoscale eddies date back at least as far as the late 1970s and early 1980s (**Supplementary Table**). Pingree et al. (1979) pioneered interdisciplinary investigations of eddies in shelf seas. Some of the first synoptic maps of phytoplankton, primary production, and seston in the open ocean were collected during the POLYMODE program, providing evidence of eddy-driven variations in all of these quantities (Radchenko 1983, Roukhiyainen & Yunev 1983). At about that same time, advances in remote sensing yielded the first satellite-based estimates of chlorophyll, indicating a variance spectrum consistent with geostrophic turbulence (Gower et al. 1980). Detailed interdisciplinary process studies of Gulf Stream Rings began in that same era, focusing on eddy-induced variability and regional impacts (Ring Group 1981). These developments led to advancements in the conceptual basis for mesoscale physical-biological interactions (Legendre & Demers 1984, Mackas et al. 1985, Woods 1988). Interest in the large-scale integrated impacts of eddies on ocean biogeochemistry was stimulated by the apparent discrepancy between estimates of new production and nutrient supply through vertical mixing (Jenkins & Goldman 1985, Shulenberger & Reid 1981). Specifically, mesoscale processes were hypothesized to be responsible for the "missing" nutrients in the subtropical gyre (Jenkins 1988a). While debate on that topic has continued through the present time, several new aspects have emerged—including the question of whether eddies constitute a net sink of nutrients in the subpolar gyre (McGillicuddy et al. 2003) and in coastal upwelling regions (Gruber et al. 2011).

This review is an attempt to synthesize our understanding of mesoscale physical-biological-biogeochemical interactions, with particular emphasis on progress over the last 15

126 years. One new development during this time period is the analysis of both data and models in
127 "eddy-centric" coordinates to illuminate the underlying dynamics; this approach is described in
128 section 2. This framework is used in section 3 as a basis to survey the mechanisms by which
129 eddies can influence upper ocean distributions of chlorophyll. Eddy impacts on mean properties
130 and fluxes are reviewed in section 4, followed by descriptions of three relatively new and
131 growing areas of inquiry: eddy-driven biological Reynolds stresses (section 5), controls on
132 community composition and diversity (section 6), and mesoscale niche utilization by higher
133 trophic levels (section 7). Concluding remarks are provided in section 8. This work builds on
134 earlier reviews by Angel and Fasham (1983), Flierl and McGillicuddy (2002), Lewis (2002),
135 Lévy (2008), Oschlies (2008), Klein and Lapeyre (2009), Williams and Follows (2011; see
136 Chapter 9). Mahadevan (2016) reviews submesoscale biological and biogeochemical dynamics.
137
138 **2. A NEW WINDOW INTO PHYSICAL-BIOLOGICAL INTERACTIONS AT THE**
139 **MESOSCALE: ANALYSIS IN EDDY-CENTRIC COORDINATES**
140   Recent progress in automated methods for identifying and tracking mesoscale eddies with
141 satellite altimetry has facilitated construction of a global atlas of eddy trajectories, amplitudes,
142 and sizes (**Figure 1**) (Chelton et al. 2011b). Use of the derived eddy-centric coordinates to
143 merge altimetric sea surface height (SSH) data with other remotely sensed properties such as
144 satellite ocean color (CHL), sea surface temperature (SST), and ocean vector winds is now
145 providing unprecedented opportunities for investigation of the physical and biological dynamics
146 of mesoscale phenomena. Construction of eddy-centric composites of many (in some cases,
147 thousands) of synoptic realizations of satellite data has allowed mean eddy-driven signals to
148 emerge. These coherent eddy-driven structures in physical and biological properties vary
149 regionally, reflecting a variety of different mechanisms by which mesoscale dynamics can
150 influence upper ocean CHL distributions (Gaube et al. 2014).
151   A key initial finding from the eddy-centric analysis of satellite-derived SSH was the degree
152 of nonlinearity of mid-ocean eddies. Whereas earlier assessments of the westward propagating
153 signal in SSH based on a single altimeter were attributed to linear Rossby wave dynamics
154 (Chelton & Schlax 1996), higher resolution data products from multiple satellite missions
155 merged together (Pascual et al. 2006) yielded a different picture. Chelton et al. (2007) computed
156 a nonlinearity parameter from the ratio of the altimetrically-inferred geostrophic swirl velocity
157 (u) to the propagation speed I of each eddy feature, finding that the vast majority of eddies were
158 nonlinear ($u/c > 1$). This finding has key implications with respect to interpretation of the
159 associated biological signal: nonlinear eddies trap fluid inside them, whereas linearly
160 propagating wavelike disturbances do not.
161   Initial investigations of the relationships between satellite-based SSH and CHL revealed
162 coherence in large-scale westward propagating signals that were attributed to linear Rossby
163 waves (Cipollini et al. 2001, Uz et al. 2001), analogous to the Chelton and Schlax (1996)
164 assessment of westward propagating signals in SSH alone. A variety of mechanisms were
165 proposed to explain the observed coherence in SSH and CHL, including (a) lateral advection of
166 the mean chlorophyll gradient, (b) uplift of the deep chlorophyll maximum into the surface layer,
167 (c) enhancement of phytoplankton biomass stimulated by upwelling of nutrients, and (d)
168 accumulation of material in convergence zones within the planetary wave field (Charria 2003,
169 Dandonneau et al. 2003, Killworth et al. 2004). These early studies focused on large-scale
170 signals characteristic of Rossby waves by processing the satellite measurements with scale-

171   selective filters, and in some cases (Killworth et al. 2004) by utilizing only a single altimeter and
172   thus a lower-resolution data set.
173   Using the new global data base of eddy trajectories, Chelton et al. (2011a) overlaid eddy
174   tracks on the westward-propagating signals previously attributed to Rossby waves in the filtered
175   SSH and ocean color data (**Figure 2d,e**). Coincidence of those features strongly suggests eddies
176   are driving the variations. How might eddies be aliased into a larger-scale Rossby wave signal?
177   Westward propagation of both types of features stems from latitudinal dependence of the effects
178   of earth's rotation, causing them to translate at approximately the same speed. In essence, a
179   patchwork of westward propagating eddies has a zonal wavenumber-frequency spectrum that is
180   qualitatively similar to that expected for linear Rossby waves, which explains why eddies can
181   pass through the filters intended to eliminate them in earlier studies (McGillicuddy 2011).
182   These findings require reassessment of the underlying mechanisms used to explain satellite
183   observations of variability in SSH and upper ocean chlorophyll. Although the same four basic
184   processes of biomass modulation (a-d) mentioned above remain valid, their expression takes
185   different dynamical forms at various scales, ranging from the mesoscale down to the
186   submesoscale (Abraham 1998, Lévy et al. 2001, Siegel et al. 2008). In the next section we
187   survey the various mechanisms, focusing on the mesoscale.
188
189   **3. SURVEY OF MECHANISMS BY WHICH EDDIES AFFECT UPPER OCEAN**
190   **CHLOROPHYLL DISTRIBUTIONS**
191
192   **3.1 Eddy Stirring**
193   Turbulent advection by mesoscale and submesoscale flows has long been recognized as a
194   source of phytoplankton patchiness in the ocean (see review by Martin (2003)). Idealized
195   models of two-dimensional geophysical flows reveal the cascade of variance from large to small
196   scales via stirring of the populations (Abraham 1998), although in some instances biological
197   dynamics can dominate (Srokosz et al. 2003). Direct observational evidence of mesoscale
198   stirring has been derived from remotely sensed synoptic snapshots of surface geostrophic
199   velocity (from altimetry) and chlorophyll (Lehahn et al. 2007). Advanced algorithms for
200   diagnosing various phytoplankton functional types has facilitated investigation of stirring effects
201   on fluid dynamical niches (d'Ovidio et al. 2010).
202   From an eddy-centric perspective, rotational flow will tend to perturb the local CHL
203   distribution via azimuthal advection. Consider, for example, a clockwise-rotating eddy (northern
204   hemisphere anticyclone) in a northward CHL gradient, shown schematically in **Figure 2a (top)**.
205   The western (leading) edge of the eddy contains a negative CHL anomaly in the northwest
206   quadrant and the eastern (trailing) edge a positive CHL anomaly in the southeast quadrant. In the
207   same background field, a counterclockwise-rotating eddy (northern hemisphere cyclone) will
208   result in a positive anomaly in the southwest quadrant and a negative anomaly in the northeast
209   quadrant (**Figure 2a, bottom**). Orientation of the dipole in CHL anomaly is a function of the
210   rotational sense of the eddy as well as the propagation direction in relation to the ambient CHL
211   field.
212   This process has been investigated in detail in the eastern subtropical South Pacific
213   (Chelton et al. 2011a). Eddies in this region (**Figure 1, "SEP"**) have a smaller mean amplitude
214   than the global average for the same latitude band (mean SSH anomaly of 3.2 cm versus 6.2 cm),
215   although their radial scale is approximately the same (110 km). As such, these eddies tend to be
216   less nonlinear than the global average, with $u/c > 1$ for 87% of them. A complex relationship

217 exists between SSH and CHL (**Figure 2c**), with eddy-driven perturbations most pronounced in
218 the areas of strongest CHL gradients. A strong mean gradient in CHL is also present in this
219 region, oriented meridionally in the western part and zonally in the eastern part in proximity to
220 the coast. Removal of the large-scale gradients and mean seasonal cycle allows the eddy signals
221 to emerge more clearly. Westward co-propagation of SSH and CHL is readily apparent, and
222 individual eddy trajectories delineate the streaks in the anomaly fields (**Figure 2d,e**).
223 Compositing the data into eddy-centric coordinates, oriented relative to the large-scale mean
224 gradient, yields dipole patterns characteristic of eddy stirring (**Figure 2b**). Although the dipole
225 structures are qualitatively similar to the theoretical prediction (**Figure 2a**) there is a subtle
226 difference: the magnitudes of the leading poles are higher in amplitude than the trailing poles.
227 This asymmetry is apparently a result of the trailing edge of the eddy interacting with an ambient
228 CHL field that has recently been under the influence of the leading edge of the eddy (Chelton et
229 al. 2011a). Similar dipole patterns emerged from an eddy-centric analysis of eddy features in the
230 Sargasso Sea (Siegel et al. 2011).
231
232 **3.2 Eddy Trapping**
233 Nonlinear eddies tend to trap the fluid contained in their interiors (Flierl 1981, Provenzale
234 1999). The composition of the trapped fluid depends on the process of eddy formation as well as
235 the local gradients in physical, chemical, and biological properties. These properties can be
236 maintained over long time periods, depending on ring evolution and exchange with the
237 surrounding water masses. Gulf Stream Rings provide a classic example (Wiebe & Joyce 1992)
238 (**Figure 3a**). Cyclonic meanders pinch off cold-core rings that trap nutrient rich, high CHL slope
239 water from the landward side of the Gulf Stream, whereas anticyclonic meanders pinch off
240 warm-core rings that trap oligotrophic low CHL water from the Sargasso Sea. A contrasting
241 example comes from the Leeuwin current (**Figure 3b**), which can spawn anticyclonic eddies
242 with enhanced CHL derived from the coastal region (Moore et al. 2007). Trapped fluid is not
243 unique to rings and boundary currents, and it is a common characteristic of nonlinear eddies in
244 the open ocean (e.g., Menkes et al. 2002).
245 The trapping mechanism is evident in eddy-centric composites from the Gulf Stream
246 region (Gaube et al. 2014). Cyclones from the region labeled "GS" in **Figure 1** contain positive
247 CHL anomalies in their interiors, and anticyclones contain negative CHL anomalies (**Figure
248 4a,b**). In both cases the anomalies appear as a monopole structure, in contrast to the dipole
249 structure produced by eddy stirring (**Figure 2b**). More importantly, these CHL anomalies are
250 present at the initial time of eddy detection (**Figure 4c,d**), suggesting they originated from the
251 process of eddy formation. Note that the region over which this analysis was performed is large
252 enough to include not only Gulf Stream rings, but also mid-ocean eddies; there is no distinction
253 between them in the eddy-centric composites. In some regimes, such as the Agulhas
254 retroflection, fluid trapped in rings can propagate well into the ocean interior, providing
255 significant lateral fluxes of physical, chemical, and biological properties Lehahn et al. (2011).
256
257 **3.3 Eddy Pumping**
258 This mechanism can be conceptualized by considering a density surface with mean depth
259 coincident with the base of the euphotic zone. This surface is perturbed vertically by the
260 formation, evolution, and destruction of mesoscale features. Three types of features are
261 schematized in **Figure 5**. Cyclones and anticyclones dome and depress the seasonal and main
262 pycnoclines, respectively. Mode-water eddies are comprised of a lens-shaped disturbance that

263 raises the seasonal pycnocline and lowers the main pycnocline. During eddy formation and
264 intensification (**Figure 5, top**), shoaling density surfaces in cyclones and mode-water eddies lift
265 nutrients into the euphotic zone, where they are rapidly utilized by the biota. Deepening of the
266 isopycnals in anticyclones pushes nutrient-depleted water out of the well-illuminated surface
267 layers. The asymmetric light field thus rectifies vertical displacements of both directions into a
268 net upward transport of nutrients. Two aspects of this process favor complete utilization of the
269 upwelled nutrients. First, the time scale for biological uptake is fast (order of days) with respect
270 to the physical supply mechanism (eddy lifetimes on the order of months). Second, because the
271 nutrient enhancement takes place in the eddy's interior, the circulation tends to isolate it from the
272 surrounding waters, which allows biomass to accumulate until the nutrients are exhausted.
273 　　　Evidence for the eddy pumping mechanism is also present in the eddy-centric anomalies
274 from the Gulf Stream region (**Figure 1, "GS"**). To begin with, the positive CHL anomaly
275 monopoles in cyclones and negative CHL anomaly monopoles in anticyclones (**Figure 4, left**)
276 are consistent with expectations based on the conceptual model for eddy pumping—although
277 monopole structures of these polarities are ambiguous with respect to eddy trapping and
278 pumping (Gaube et al. 2014). As stated above, the presence of these anomalies at the time of
279 first detection is consistent with trapping. However, the signature of eddy pumping is manifested
280 by a subtle trend that barely exceeds the associated uncertainties: as cyclones intensify in the first
281 twelve weeks of their lifetimes (**Figure 4c**), CHL anomalies also increase (**Figure 4d**). In
282 contrast, the negative CHL anomaly in anticyclones is more stable over time during the same
283 interval.
284 　　　It is important to note that the eddy-centric analysis based on sea level cannot distinguish
285 between mode-water eddies and regular anticyclones. Because steric height in mode-water
286 eddies is dominated by downward displacement of the main pycnocline, they appear as positive
287 anomalies in sea level, indistinguishable from regular anticyclones both in terms of SSH and
288 their rotational velocities (McGillicuddy et al. 2007, Sweeney et al. 2003). As such, CHL
289 anomalies generated by eddy stirring are expected to be the same in mode-water eddies as they
290 are in regular anticyclones. In contrast, the expected response in terms of eddy pumping is
291 confounding: positive for intensifying mode-water eddies and negative for intensifying regular
292 anticyclones. As for trapping, the CHL signature would depend on the ambient gradients and
293 whether the mechanism of formation was subduction from a remote source (Ebbesmeyer &
294 Lindstrom 1986) or local generation through eddy-wind interaction (McGillicuddy 2015).
295 　　　The eddy-induced vertical flux depends not only on the structure of the isopycnal
296 displacements, but also on the sense in which they are being perturbed by eddy dynamics. The
297 latter characteristic is determined by the eddy's developmental stage, as well as eddy-eddy
298 interactions during its lifetime. During the process of eddy decay (**Figure 5, bottom**), the sense
299 of the vertical motions is opposite to that during formation/ intensification: relaxation of the
300 density perturbations associated with eddy decay results in upper ocean downwelling in cyclonic
301 features and mode-water eddies, while causing upwelling within anticyclones. An excellent
302 example of the latter is provided by frictional spindown of warm core rings. A model by Franks
303 et al. (1986) demonstrated how phytoplankton biomass enhancement could result from the
304 nutrient input caused by the approximately 1 m day^{-1} vertical velocities at ring center. Uptake
305 rates of nitrate and silicic acid observed in the same ring which were sufficient to utilize the
306 upward flux of nutrients (Nelson et al. 1989).
307

3.4 Eddy-wind interaction

It was recognized long ago that the superposition of a wind-driven Ekman flow on a mesoscale velocity field gives rise to ageostrophic circulations involving significant vertical transports (Niiler 1969, Stern 1965). Submesoscale patches of vertical velocity result from the generalized Ekman divergence, which includes vortex stretching terms associated with advection of the interior vorticity by the boundary layer velocity. For a uniform wind stress applied to a radially symmetry eddy, this effect creates a dipole of upwelling and downwelling, the structure of which depends on the direction of the wind and the vorticity of the eddy (see Figure 4.33 of Flierl and McGillicuddy, 2002).

The presence of mesoscale variability in the ocean affects the wind stress itself, via two different processes. First, there is a feedback from sea surface temperature. Cooler ocean temperatures tend to stabilize the marine atmospheric boundary layer (MABL), decoupling it from winds aloft; conversely, warmer ocean temperatures tend to destabilize the MABL thereby decreasing vertical shear in the wind. The net effect is to increase surface wind speeds over warmer water and decrease them over colder water, leading to measurable differences in wind stress, its curl, and therefore Ekman pumping (Chelton et al. 2004). Second, there is a direct effect on the stress due to eddy-driven surface currents. That is, higher stress occurs on the flank of the eddy where the wind opposes the surface current, with lower stress on the flank of the eddy where the wind and the current are in the same direction (**Figure 6a**). The net result is Ekman suction (upwelling) in the interiors of anticyclones (**Figure 6b**) (Dewar & Flierl 1987, Martin & Richards 2001), and Ekman pumping (downwelling) in the interiors of cyclones (Gaube et al. 2013). In contrast to the prior two mechanisms of eddy-wind interaction, the vertical velocity field resulting from eddy-induced Ekman pumping is a monopole located at eddy center that does not depend on the direction of the wind.

Gaube et al. (2015) assessed the relative magnitudes of these three processes, finding that the sea surface temperature effect is generally smaller than the other two. Magnitudes of the vertical velocities induced by vorticity advection tend to be larger than those arising from eddy-induced Ekman pumping. However, the integrated impact depends critically on the structure of the associated vertical velocity fields. Specifically, the relative persistence of the monopole generated by the surface current stress effect overshadows the constantly-fluctuating dipole created by vorticity advection (see Gaube et al. (2015), Figures 8 and 9).

In nutrient limited conditions, eddy induced Ekman pumping is thus expected to produce positive CHL anomalies in anticyclones (upwelling), and negative CHL anomalies in cyclones (downwelling). This is precisely the pattern observed in eddy-centric composites of CHL anomaly and eddy induced Ekman pumping from the South Indian Ocean (**Figure 4e,f**). Time-series of CHL anomaly (**Figure 4g,h**) reveal CHL anomalies are present at the time of eddy detection, suggesting the eddy trapping mechanism is also at work. Indeed, both satellite data and *in situ* process studies (Moore et al. 2007, Waite et al. 2007) have shown that high-chlorophyll waters of coastal origin can be entrained into anticyclones of the Leeuwin Current (**Figure 3b**). However, the time series presented in **Figure 4g,h** also show that the positive CHL anomalies in anticyclones are significantly higher in weeks 6-11 as compared with weeks 1-4, which is consistent with eddy-induced Ekman pumping. Martin and Richards (2001) cited this process as a potential contributor to nutrient flux in an anticyclone in the northeast Atlantic. Eddy-induced Ekman pumping has also been invoked as an explanation for an extraordinary bloom of diatoms deep in the euphotic zone of a mode-water eddy in the Sargasso Sea

353 (McGillicuddy et al. 2007) as well as near-surface CHL variations in the South China Sea (Li et
354 al. 2014).
355
356 **3.5 Impacts on mixed layer depth**
357   The presence of geostrophic motions and their associated vorticity produces local
358 variations in the effective Coriolis frequency, which can affect propagation characteristics of
359 near-inertial waves (e.g., Kunze 1985). Regions of negative vorticity can focus and amplify of
360 such waves, thereby augmenting shear, potentially leading to increased vertical mixing.
361 Simulations by Klein and Hua (1988) illustrated the mesoscale heterogeneity in mixed layer
362 depth that can arise from this process in a quasigeostrophic flow field forced by a uniform wind.
363 This "inertial Ekman pumping" creates a broad spectrum of variations in mixed layer depth,
364 although an eddy-scale signal is prominent.
365   Mixed layer depth is also modulated by the local changes in stratification driven by eddy-
366 induced vertical isopycnal displacements. For example, in a cyclonic eddy, upward doming of
367 the pycnocline increases stratification in the upper ocean, thereby shallowing the mixed layer
368 depth for a given amount of turbulent kinetic energy from the surface. Conversely, downward
369 deflection of the pycnocline by an anticyclonic eddy tends to reduce upper ocean stratification,
370 thereby allowing the same amount of turbulent kinetic energy to create a deeper mixed layer.
371 These direct impacts of the local stratification tend to be augmented by air-sea heat flux
372 anomalies resulting from the associated perturbations in sea surface temperature (Williams
373 1988). For example, consider a situation in which the mean SST is such that there is no net
374 sensible heat transfer to or from the atmosphere. Cold sea surface temperature anomalies in
375 cyclones tend to draw heat into the ocean from the atmosphere, further increasing stratification in
376 those features relative to the ambient waters. Similarly, warm sea surface temperature anomalies
377 in anticyclones tend to release heat from the ocean into the atmosphere, cooling the surface
378 ocean and thereby enhancing convection. The tendency for anticyclonic eddies to have deeper
379 mixed layers than cyclones has been noted in the Gulf Stream (Dewar 1986), the northeast
380 Atlantic (Williams 1988), the North Pacific (Kouketsu et al. 2012), and the South Indian Ocean
381 (Dufois et al. 2014, Gaube et al. 2013). In fact, Dufois et al. (2014) have offered deeper mixed
382 layers (**Figure 7**) as an alternative explanation for long-lived CHL anomalies in anticyclones of
383 the South Indian Ocean (**Figure 4e-h**). Differentiating between enhanced mixing and eddy-
384 induced Ekman pumping is difficult in this case, as both mechanisms tend to produce CHL
385 anomalies of the same sign in this nutrient-limited regime. In a light-limited regime, eddy-driven
386 variations in mixed layer depth would presumably produce the CHL anomalies of the opposite
387 sign: shallower (deeper) mixed layers in cyclones (anticyclones) would lend themselves to higher
388 (lower) CHL (**Table 1**).
389
390 **3.6 Mechanisms of CHL enhancement in the peripheries of anticyclonic eddies**
391   In contrast to the dipole and monopole anomalies of CHL described above, annular ring-
392 shaped patterns have been observed around the peripheries of eddies, particularly anticyclones.
393 Although such patterns have yet to emerge in eddy-centric composites of many eddies, synoptic
394 snapshots have revealed these features in a variety of regimes, including the Southern Ocean
395 (Kahru et al. 2007) (**Figure 8, top**), the Gulf of Alaska (Mizobata et al. 2002), and the
396 Mozambique channel (José et al. 2014). Qualitatively similar patterns have been produced in a
397 variety of models (José et al. 2014, Lapeyre & Klein 2006, Lévy & Klein 2004, Lima et al. 2002,
398 Mahadevan et al. 2008) (**Figure 8, bottom**). Two basic mechanisms have been invoked to

399　explain these annular patterns: (1) lateral entrainment of streamers of high-CHL water from
400　nearby coastal or frontal regions, and (2) local enhancement via either stratification in light-
401　limited systems or nutrient supply via upwelling along the eddy periphery. The latter can arise in
402　submesoscale patches of upwelling and downwelling associated with meandering of the circular
403　front that delineates the outer edge of an eddy (McGillicuddy et al. 1995). Upwelling rates in
404　such features can be as high as 10-100 m d^{-1} as a result of eddy-wind, eddy-eddy, and/or eddy-
405　front interactions (Mahadevan et al. 2008, Martin & Richards 2001, Yoshimori & Kishi 1994).
406　　　　These upwelling rates that occur at the submesoscale are much larger than those
407　characteristic of the eddy-scale itself.   However, these intense vertical motions are also
408　associated with swift horizontal currents characteristic of frontal regions. As such, a water parcel
409　transported into the euphotic zone by a submesoscale upwelling cell can be rapidly advected into
410　a submesoscale downwelling cell where that same parcel can be transported back out of the
411　euphotic zone. The degree to which the upwelled nutrients will be utilized by the biota depends
412　on the relative time scales of the supply and uptake processes. This is of course a function of
413　the dynamical regime and the local chemical and biological environment (see review by
414　Williams and Follows (2003)). Another key factor is the degree of reversibility along the
415　upwelling and downwelling trajectory. Both vertical mixing and lateral dispersion can lend a
416　degree of irreversibility to the process, making the nutrient content of the downwelled water less
417　than that which was upwelled, resulting in a net transport of nutrients (Martin & Richards 2001,
418　Martin et al. 2001).
419
420　**3.7 Global perspective**
421　　　　The preceding sections (3.1-3.6) illustrate the variety of mechanisms by which eddies can
422　shape CHL distributions in the upper ocean. A global perspective is facilitated by examination
423　of the correlation between satellite measurements of SSH and CHL (**Figure 9**). Areas of positive
424　correlation are indicative of positive CHL anomalies associated with anticyclonic eddies
425　(positive SSH anomaly) and negative CHL anomalies with cyclonic eddies (negative SSH
426　anomaly). Conversely, regions of negative correlation are indicative of positive CHL anomalies
427　associated with cyclonic eddies, and negative CHL anomalies associated with anticyclones. The
428　coherent regional structure in this correlation strongly suggests systematic variations in the
429　mechanisms of mesoscale physical-biological interactions in the global ocean (Gaube et al.
430　2014).
431　　　　A prime example of negative correlation occurs in the Gulf Stream region. Eddy-centric
432　analysis (**Figure 4a-d**) suggests both trapping (**Figure 3a**) and eddy pumping (**Figure 5**) are at
433　work. Negative correlation is observed in other western boundary current systems and their
434　midlatitude extensions, including the Kuroshio Current, the Agulhas Current and Brazil-
435　Malvinas Confluence. Similarly, most eastern boundary current systems, such as the California
436　Current, the Peru-Chile Current and the Benguela Current are characterized by negative
437　correlation. Regions of negative correlation are also observed in the open ocean, such as
438　northeast of Madagascar and to the east of the Hawaiian Islands in the North Pacific.
439　　　　A prominent feature of positive correlation resides in the South Indian Ocean. Eddies in
440　this region exhibit the signature of trapping, likely associated with high-CHL anticyclones and
441　low-CHL cyclones spawned from the Leeuwin Current (**Figure 3b; Figure 4h**). High CHL in
442　anticyclones and low CHL in cyclones may be maintained by (a) eddy induced Ekman pumping
443　(**Figure 4e,f**) and/or (b) eddy impacts on mixed layer depth (**Figure 7**). These same mechanisms
444　may be operating in other regions of positive correlation, such as the central South Pacific,

445 subtropical North and South Atlantic and around the Hawaiian Islands in the central North
446 Pacific.
447   The SSH-CHL cross-correlation along the line in the southeast Pacific (**Figure 9**)
448 examined by Chelton et al. (2011b) is consistent with **Figure 2f**, with negative values in the east
449 and positive values in the west. However, the key to diagnosis of the eddy stirring characteristic
450 of the region (**Figure 2a,b**) lies in the time-lagged cross correlation. Maximum positive
451 correlation occurs with SSH anomaly lagging CHL anomaly by approximately one month,
452 whereas maximum negative correlation occurs with SSH anomaly leading CHL anomaly by one
453 month (**Figure 2f**). This is a result of the westward propagating dipoles, in which positive and
454 negative lobes of CHL anomalies are offset from eddy center where the extrema in SSH occur.
455 Note that the negative correlation at -1 month lag tends to be weaker than the positive correlation
456 at +1 month lag, owing to the fact that the ambient CHL on the trailing edge of the eddy has been
457 previously disturbed by advection from the leading edge (Cf. **Figure 2b**).
458   In aggregate, these results highlight the utility of eddy-centric compositing to illuminate
459 mechanisms of physical-biological interaction. However, limitations are also clear. For
460 example, based on this information alone, a CHL response to upwelling / downwelling occurring
461 during eddy intensification cannot be differentiated from the trapping of CHL during eddy
462 formation in regions where the ambient CHL gradient favors enhanced (suppressed) CHL in the
463 interiors of cyclonic (anticyclonic) eddies (e.g. the Gulf Stream). Likewise, a CHL response to
464 eddy-induced Ekman pumping and/or eddy-driven perturbations to mixed layer depth cannot be
465 differentiated from the trapping of CHL in regions where the ambient CHL gradient favors
466 enhanced (suppressed) CHL in the interiors of anticyclonic (cyclonic) eddies (e.g. the South
467 Indian Ocean). The temporal evolution of the SSH and CHL signatures of eddies can help to
468 address these ambiguities, but unequivocal diagnosis of the underlying mechanisms is not
469 possible on the basis of satellite data alone. Moreover, the near-surface manifestation of
470 mesoscale eddies in ocean color data may not always reveal the physical-biological dynamic in
471 its entirety, insofar as large amplitude biological responses can take place deep in the euphotic
472 zone where they are only partially detected by satellite (McGillicuddy et al. 2007). Thus, in
473 order to develop a more complete understanding of the role of mesoscale eddies in upper ocean
474 ecosystem dynamics and biogeochemical cycling, detailed analysis of satellite observations
475 together with subsurface *in situ* measurements and numerical simulations is needed.
476
477 **4. EDDY IMPACTS ON MEAN PROPERTIES AND FLUXES**
478   Whereas the study of eddy-driven variability is guided by observations, quantification of
479 their integrated impact on mean properties of the system and associated biogeochemical fluxes
480 ultimately relies on models. A wide variety of approaches have been used to address this
481 question, ranging from idealized process-oriented formulations to more realistic simulation-
482 oriented configurations. These approaches are complementary in a number of ways, not the least
483 of which is that the former provide conceptual frameworks for diagnosis of more complex
484 simulations. For example, Lee and Williams (2000) evaluated eddy-driven fluxes in a periodic
485 channel forced with wind stresses and heat fluxes that mimic subtropical to subpolar
486 environments. Adopting the Gent et al. (1995) formalism, they derive eddy-induced advection
487 and diffusion from the time-averaged and zonally-averaged tracer equations. Their results show
488 that eddy-induced advection and diffusion of nutrients oppose each other in the upper ocean,
489 whereas they reinforce each other in the deep ocean (**Figure 10a**). Wind-driven flows also play
490 an important role in the near-surface layer (**Figure 10b**): lateral Ekman fluxes into the

491 subtropical gyre oppose the outward eddy-induced advection, and downwelling of nutrients
492 driven by Ekman convergence counters upward eddy-induced advection (eddy pumping).
493 Idealized models have also elegantly demonstrated that resolving mesoscale eddies may not be
494 adequate for assessing the mean fluxes. Lévy et al. (2001) simulated frontal instability at
495 resolutions of 10, 6, and 2 km, finding that new production systematically increased with
496 resolution. Productivity of the 2 km model was almost a factor of three higher than the 10 km
497 model, clearly demonstrating the importance of submesoscale processes.
498   It is only relatively recently that truly eddy-resolving models have been run on basin to
499 global scales (Hecht & Hasumi 2008), and computational limitations generally preclude
500 simulations much longer than 5-10 years for coupled physical-biological-biogeochemical
501 applications. Such integrations are typically long enough to provide several years of quasi-
502 equilibrium solution for analysis subsequent to the transients associated with adjustment to initial
503 conditions. However, these solutions can be far from true equilibrium, as illustrated in a recent
504 study by Lévy et al. (2012b) comparing the results of 1/54º and 1/9º resolution models integrated
505 for 50 years in an idealized double-gyre simulation reminiscent of the North Atlantic (**Figure
506 11**). After 50 years, the two models show systematic regional differences in total production of
507 ±60%. A particularly salient feature of the higher resolution model is a ~30% decrease in
508 productivity of the subtropical gyre, attributed to a long-term deepening of the nitracline in that
509 region. In other words, mesoscale and submesoscale dynamics produce not only local
510 fluctuations, but also changes in the mean state of the system. This caveat must be kept in mind
511 when interpreting the results from shorter-term integrations described below.
512
513 **4.1 Subtropical Gyre**
514   The role of eddies in supplying nutrients in the subtropical gyre has been debated for
515 some time. Comparison of two hydrographic profiles sampled one month apart off Bermuda
516 documented an apparently eddy-driven nutrient injection event that could account for 20-30% of
517 the annual new production (Jenkins 1988b). High-resolution transects in the Pacific (Venrick
518 1990) and Atlantic (Strass 1992) revealed mesoscale variations in chlorophyll consistent with
519 eddy-induced upwelling. Surveys of a cyclone in the lee of Hawaii documented increased
520 primary production in its interior, and extrapolation of that result suggested a 20% enhancement
521 of global primary production by mid-ocean eddies (Falkowski et al. 1991). A variety of models
522 have been brought to bear on this question, but the magnitude of the eddy-induced flux and its
523 utilization is model-dependent (Eden & Dietze 2009, Martin & Pondaven 2003, McGillicuddy et
524 al. 2003, McGillicuddy et al. 1998, McGillicuddy & Robinson 1997, Oschlies 2002, Oschlies &
525 Garcon 1998, Pasquero et al. 2005).
526   An example is provided in **Figure 12**, in which the horizontal and vertical nutrient fluxes
527 in a one-tracer light-limited nutrient transport model have been decomposed into their time-mean
528 and eddy-driven components. Although this decomposition is different from that used by Lee
529 and Williams (2000) to distill **Figure 10**, some commonalities are evident in the results. In the
530 subtropical gyre, mean vertical advection constitutes a sink of nitrate, owing to the downwelling
531 caused by Ekman convergence. Eddy-induced vertical advection is a source of nitrate, which is
532 sufficient to overcome the mean downward transport such that the total vertical advection is a net
533 source of nitrate. Note that Lee and Williams (2000) predicted the opposite, with Ekman
534 downwelling overshadowing eddy pumping (**Figure 10b**). In other aspects, the realistic
535 simulation is more similar to the idealized model. Horizontal advection (**Figure 12**) is near zero
536 over much of the subtropical gyre due to the low concentration of nitrate in the surface waters of

537   this region. However, horizontal advection is a net source of nutrients along the northern edge of
538   the gyre. This lateral flux of nitrate into the gyre arises mostly from the mean fields, roughly
539   consistent with the Ekman flux of nitrate described by Williams and Follows (1998).
540
541   **4.2 Subpolar Gyre**
542   New production in the subpolar gyre is considerably higher than that in the subtropical
543   gyre (**Figure 12**), due to a combination of vigorous vertical mixing and mean upwelling from
544   divergence of the wind-forced Ekman surface current. Interestingly, the time-varying
545   component of vertical advection is negative over a large portion of this region, especially in areas
546   where the wintertime mixed layer depth is deepest. In the southern part of the gyre, the
547   magnitude of this sink is sufficient to overcome the mean upward vertical advection, causing the
548   total vertical advection to be negative in that area. Horizontal advection is also important in this
549   region. The large area of negative net lateral flux arises primarily from mean horizontal
550   advection. Eddy-driven horizontal advection in this area varies on smaller scales but generally
551   tends to reinforce the mean. This negative lateral flux is due to northeastward flow of the North
552   Atlantic importing lower concentrations of nitrate into the subpolar gyre.
553   In contrast to the subtropical gyre where eddy-driven fluxes constitute a net source of
554   nutrients, it appears that the oceanic mesoscale has a significant impact on nutrient removal from
555   the euphotic zone in the subpolar gyre. A similar feature is evident in the simulations of Oschlies
556   (2002), suggesting this result is not model dependent. Diagnosis of the solutions shown in
557   **Figure 12** suggests that the downward nutrient flux results from mesoscale processes associated
558   with restratification following deep convection (**Figure 13**). Indeed, mesoscale and
559   submesoscale dynamics have been shown to play a key role in the process of restratification
560   (Mahadevan et al. 2012, Marshall 1997, Nurser & Zhang 2000). Lévy et al. (1998, 1999)
561   described how mesoscale restratification increases productivity following convection by
562   releasing phytoplankton from light limitation. The eddy-induced nutrient sink shown in **Figure
563   13** is the counterpart to that process deeper in the water column: the same mesoscale dynamics
564   that restratify the near-surface region pump nutrients out of the euphotic zone. This removal
565   takes place at a time when the ambient nutrients are in excess of limiting concentrations, so there
566   is no immediate reduction of productivity. However, this process would tend to decrease
567   productivity on seasonal to annual time scales, insofar as a portion of the nutrients brought into
568   the euphotic zone by wintertime mixing are pumped back downward prior to utilization. On the
569   other hand, Mahadevan et al. (2012) have suggested that the mixed layer eddies involved in
570   restratification could increase overall productivity.
571
572   **4.3 Coastal upwelling systems**
573   Upwelling regions along coastal margins support some of the most productive marine
574   ecosystems on earth. These systems also tend to have high eddy kinetic energy, owing to the
575   squirts, jets, filaments, and eddies that are formed when along-shore wind stress generates an
576   Ekman divergence at the coast that leads to upwelling. In contrast to the oligotrophic waters of
577   the open ocean where eddy-induced nutrient fluxes can increase productivity, it appears that
578   eddy-driven processes decrease productivity in eastern boundary upwelling systems (Gruber et
579   al. 2011). Two mechanisms appear to be at work: lateral stirring and subduction.
580   First, stirring by mesoscale structures transports upwelling-derived biomass offshore,
581   thereby reducing biomass in the upwelling zone itself. This process was noted by Rossi et al.
582   (2008) in their analysis of Finite Size Lyapunov Exponents (FSLEs) and chlorophyll

583   distributions in the Benguela and Canary upwelling systems. FSLEs provide a measure of lateral
584   stirring, and can be computed directly from satellite altimeter data. Rossi et al. found that
585   chlorophyll concentration was inversely correlated with FSLEs in these systems, such that the
586   more vigorous stirring in the Benguela system was associated with lower chlorophyll
587   concentrations than the Canary system. The role of mesoscale processes in reducing
588   phytoplankton biomass was quantified in a model of the Benguela system, indicating eddy-
589   driven transports are responsible for 30-50% of the offshore fluxes of biological tracers
590   (Hernández-Carrasco et al. 2014).
591   The second mechanism involves offshore subduction of upwelled nutrients. Gruber et al.
592   (2011) diagnosed the eddy-induced nitrogen fluxes from a high-resolution coupled-physical
593   biological model of the California Current system (**Figure 14**). As expected, vertical eddy-
594   induced fluxes are positive close to the coast, where mesoscale dynamics are intimately involved
595   in the upwelling process. Lateral eddy fluxes transport nitrogen away from the coast in the
596   surface layer, in concert with downward eddy-induced transport offshore—the net result of
597   which is subduction into the ocean interior. These subducted nutrients occupy an intermediate
598   layer that is distinct from that which feeds the Ekman-driven upwelling cell, thus constituting a
599   "leak" of nutrients that decreases the overall productivity of the system.
600   In addition to eddy-induced transports, there are special biogeochemical transformations
601   that take place within eddies in upwelling systems. For example, hotspots for fixed-nitrogen loss
602   have been observed in association with anticyclonic eddies in the Peru oxygen minimum zone
603   (Altabet et al. 2012, Bourbonnais et al. submitted, Stramma et al. 2013). However, observations
604   of this process are currently so sparse that quantification of their integrated impact on nutrient
605   budgets is not yet possible.
606
607   **4.4 Other regional Studies**
608   Growing awareness of the diversity of eddy impacts on biological systems has led to
609   increasing numbers of regional studies. For example, analysis of satellite-based observations of
610   sea level and ocean color in the Weddell-Scotia confluence in the Southern Ocean indicates that
611   cyclonic eddies enhance biological production (Kahru et al. 2007).   Both observations and
612   models suggest anticyclonic eddies enhance production in the northern Gulf of Alaska, by virtue
613   of the iron they transport from the coastal margin into the interior (Crawford et al. 2007, Xiu et
614   al. 2011). A high-resolution model of the South China Sea suggests cyclonic eddies are an
615   important source of nutrients to the surface ocean in that region, triggering shifts in
616   phytoplankton species composition toward diatoms, thereby increasing export flux and
617   associated cycling of carbon (Xiu & Chai 2011). On the other hand, observations in the South
618   China Sea have revealed enhanced export fluxes in anticyclones, attributed to submesoscale
619   upwelling along eddy peripheries (Zhou et al. 2013; Cf. section 3.6). Using data from shipboard
620   surveys, Prasanna Kumar (2007) estimated that eddy pumping increases productivity in the Bay
621   of Bengal by a 50-100%. In a model of the Arabian Sea, Resplandy et al. (2011) found that
622   multiple mesoscale processes contributed to regional nutrient budgets, namely (1) lateral
623   advection from coastal upwelling zones into the interior via jets and filaments, (2) eddy
624   pumping, and (3) eddy-driven restratification following monsoonally-driven convective mixing.
625   Such integrative analyses seeking to assess the net impact of eddies on various systems draw
626   heavily on the growing data base provided by *in situ* process studies (**Supplementary Table**).
627

5. EDDY-DRIVEN BIOLOGICAL REYNOLDS STRESSES

Three-dimensional coupled physical-biological models are typically formulated in terms of the mean field approximation, in which properties φ_i in a given grid cell are assumed to be adequately represented by their mean value $\overline{\varphi_i}$. Of course, fluctuations φ_i' exist; the Reynolds decomposition expresses the full field as a sum of mean and fluctuating components, the latter of which average to zero: $\varphi_i = \overline{\varphi_i} + \varphi_i'$. Biological and biogeochemical transformations typically involve nonlinear functions, so even though $\overline{\varphi_i'} = 0$, the average value of such a function operating on the fluctuations $\overline{f(\varphi_i')}$ does not necessarily vanish. Moreover, the average product of two constituents $\overline{\varphi_i \varphi_j}$ includes contributions not only from the means $\overline{\varphi_i}\,\overline{\varphi_j}$ but also from the "biological Reynolds stresses" $\overline{\varphi_i' \varphi_j'}$. These effects have been examined in a variety of idealized frameworks, including theoretical (Goodman 2011, Goodman & Robinson 2008), one-dimensional (Brentnall et al. 2003), and two-dimensional (Wallhead et al. 2008), providing quantification of the limitations of the mean field approximation in such systems.

It is only recently that the net impact of fluctuations in biological properties has been examined in three-dimensional simulations of mesoscale and submesoscale turbulence (e.g., Wallhead et al. 2013). Lévy and Martin (2013) diagnosed these terms from their 1/54° resolution physical-biological model of the North Atlantic, making the distinction between "eddy reactions" and "eddy transports" of the type described in earlier sections. Their findings illustrate the eddy reaction terms play qualitatively different roles for different state variables (see Lévy and Martin's Figure 9). For nitrate, the eddy reactions are generally small relative to the mean biogeochemical reactions, with the latter being balanced by a complex latitudinally-dependent combination of vertical mixing, mean advection, and eddy transport. In contrast, eddy reactions are amongst the largest terms in the phytoplankton equation, negative in sign and varying inversely with the mean reaction term. In other words, nonlinear interactions at the mesoscale and submesoscale reduce primary productivity. For zooplankton, the eddy reactions vary with latitude: they are small south of 28ºN, increase secondary productivity between 28ºN and 40ºN, and decrease secondary productivity north of 40ºN. Although the details of these diagnoses may be model dependent, these findings clearly illustrate that eddy-driven fluctuations can be rectified by nonlinear biogeochemical transformations—and that the magnitudes of the eddy reactions are on the order of 5-15% of the means (see Lévy and Martin's Figure 7). Whereas complete knowledge of a modeled system lends itself to relatively straightforward computation of biological Reynolds stresses, observational assessment is made more challenging by the lack of multiscale resolution of all relevant quantities. Initial attempts to quantify eddy-driven biological Reynolds stresses suggest more modest magnitudes than those derived from models (Martin et al. submitted).

6. INFLUENCES ON PHYTOPLANKTON COMMUNITY COMPOSITION AND DIVERSITY

Eddy-induced disturbances in the physical and chemical environment can bring about changes in the communities of primary producers. In fact, such biological responses may regulate the net impact on biogeochemical fluxes described above. For example, Goldman (1988) suggested the "spinning wheel" concept in which the background state of oligotrophic systems is dominated by small phytoplankton growing primarily on nutrients that are recycled through the microbial loop. This state is episodically perturbed by the input of nutrients to the base of the euphotic zone, causing a shift in phytoplankton species composition from picoplankton toward much larger cells such as diatoms. In such a scenario, these large cells

674 would sink rapidly once the nutrient enhancement was depleted, thereby contributing a
675 disproportionately large fraction of new versus total primary production. Laboratory culture
676 experiments have confirmed that diatoms can grow rapidly enough to produce significant blooms
677 even at the low light levels characteristic of the base of the euphotic zone (Goldman &
678 McGillicuddy 2003). Indeed, evidence for mesoscale variations in diatom abundance has been
679 observed in a variety of oceanographic environments, including the North Pacific (Brzezinski et
680 al. 1998), Hawaiian lee eddies (Olaizola et al. 1993, Seki et al. 2001, Vaillancourt et al. 2003),
681 the Hawaiian Ocean Time-series (Letelier et al. 2000), the Sargasso Sea (Krause et al. 2010,
682 McGillicuddy et al. 2007), and the Bermuda Atlantic Time-series (Krause et al. 2009, McNeil et
683 al. 1999, Sweeney et al. 2003). Bibby and Moore (2011) found that the response of diatom
684 populations to eddy-induced upwelling in the subtropical Atlantic and Pacific depends on the
685 nitrate to silicate ratio of the upwelled water. In several cases, mesoscale diatom blooms have
686 been linked directly to enhanced export (Allen et al. 2005, Benitez-Nelson et al. 2007, Bidigare
687 et al. 2003).
688   Even more general relationships between the mesoscale environment and plankton
689 community structure have emerged from both observations and models. For example, Rodriguez
690 et al. (2001) identified a linear relationship between the size-abundance spectrum (SAS) of
691 phytoplankton and vertical velocity in the northwestern Alboran Sea. Specifically, upwelling
692 (downwelling) motions tended to increase (decrease) the relative abundance of large
693 phytoplankton, thereby flattening (steepening) the SAS—suggesting that mesoscale motions
694 exert a primary control on size structure of phytoplankton communities.
695   Models have been used to address a growing interest in the influence of mesoscale
696 dynamics on the diversity of open ocean phytoplankton populations, challenging the assumption
697 of environmental homogeneity in Hutchinson's (1961) classic "paradox of the plankton." Using
698 a two-species model with a uniform distribution of limiting resource embedded in
699 quasigeostrophic turbulence, Bracco et al. (2000) show how coherent vortices can preserve
700 diversity by isolating populations from the surrounding fluid: a less-fit species can persist in
701 conditions in which they would otherwise be outcompeted if the more-fit species were not
702 excluded by the lack of mixing. Perruche et al. (2011) considered a case in which the mesoscale
703 motions influenced the distribution of resources (nutrients), finding that surface quasigeostrophic
704 turbulence facilitated coexistence of two competing phytoplankton species. Upwelling in
705 filaments stimulated both species, whereas eddy cores serve as refugia as found by Bracco et al.
706 (2000).
707   Additional studies of phytoplankton diversity have been facilitated by the development of
708 the so-called "Darwin" model in which many tens of species ("ecotypes") are stochastically
709 assigned physiological characteristics with basic allometric tradeoffs (Follows et al. 2007). By
710 allowing the suite of ecotypes to compete in a three-dimensional model ocean, phytoplankton
711 species composition is an emergent property of the system. Clayton et al. (2013) examined an
712 eddy-permitting case, finding that regions of high eddy kinetic energy in western boundary
713 currents coincide with high diversity in the simulated phytoplankton community (**Figure 15a**).
714 These "hotspots" in diversity are supported by the confluence of multiple upstream populations,
715 local stimulation via nutrient supply, and environmental variability provided by eddies. Lévy et
716 al. (2014) quantified the impact of dispersal on diversity by applying the Darwin biological
717 module into eddy-resolving simulations in an idealized North Atlantic domain (depicted in
718 **Figure 11a**). Their counterintuitive results (**Figure 15b**) suggest that increasing dispersion leads
719 to increasing local diversity (order 10-100 km scales) and decreasing regional diversity (order

720   1000 km scales). In other words, hydrodynamic transport leads to the dominance of fewer
721   species overall, but those fewer species occur over larger ranges with a higher degree of
722   coexistence. Studies of this type are still quite novel, and the data needed to test such models is
723   only beginning to emerge (Clayton et al. 2014, Follows et al. 2007).
724
725   **7. EFFECTS ON HIGHER TROPHIC LEVELS**
726   Eddy dynamics can perturb oceanic ecosystems, influencing trophic levels ranging from
727   primary producers (as described in section 6) to top predators. For example, Wiebe and Flierl
728   (1983) described changes in zooplankton (euphausiid) species distributions during the decay of a
729   cold core ring: native cold water species such as *Nematoscelis megalops* emigrated, whereas
730   warm water species such as *Stylocheiron carinatum* immigrated. These changes in distributional
731   patterns were facilitated by vertical positioning behavior in the presence of a hydrodynamic
732   environment that varies with depth. Specifically, descent of the *N. megalops* population during
733   ring decay resulted in its exit from the region of trapped fluid, thereby bringing about
734   expatriation. In contrast, the near-surface keeping behavior of *S. carinatum* subjects it to
735   enhanced horizontal mixing within the mixed layer, thereby facilitating its invasion into the ring
736   interior. Active vertical positioning also supports a mechanism for concentrating organisms
737   within a mesoscale flow field: depth-keeping behavior in the presence of convergence (Genin et
738   al. 2005, Olson & Backus 1985).
739   Mesoscale phenomena are also relevant to the transport and survival of planktonic larvae.
740   Lobel and Robinson (1986) noted a cyclonic eddy near Hawaii retained larval reef fishes for a
741   time period sufficient to complete their pelagic developmental phase and resettle their native
742   reefs. On the other hand, eddies also provide means for enhanced larval dispersion and
743   population connectivity, both in the coastal margin (Mitarai et al. 2009) and in the deep sea
744   (Adams et al. 2011). Bakun (2006) presented a conceptual framework in which eddy-driven
745   variations in productivity offer competing tradeoffs in terms of larval survival: enhanced
746   productivity improves early life nutrition at the expense of increased predator abundance,
747   whereas suppressed productivity decreases the abundance of predators at the expense of poorer
748   larval nutrition. These concepts have been invoked to explain mesoscale variations in the
749   distribution of larval bluefin tuna (Alemany et al. 2010, Lindo-Atichati et al. 2012), sailfish,
750   marlin, swordfish, and other species (Richardson et al. 2010).
751   Distributions of adult fishes have also been associated with the mesoscale environment.
752   Based on catch data, cyclonic eddies appear to be home to higher abundances of bluefin tuna in
753   the Gulf of Mexico (Teo & Block 2010) and blue marlin in the vicinity of Hawaii (Seki et al.
754   2002). Based on acoustic and trawl surveys, mid-water fishes are associated with anticyclonic
755   eddies in the Iceland Basin (Godø et al. 2012). Visual sightings of cetaceans (whales and
756   dolphins) in the northern Gulf of Mexico indicated congregations in or near cyclones and in the
757   confluence of cyclone-anticyclone pairs where zooplankton and micronekton prey abundances
758   were higher (Davis et al. 2002). Seabirds of various kinds have been associated with the
759   peripheries of eddies and convergence zones between them, including great frigate birds in the
760   Mozambique channel (Tew Kai & Marsac 2010, Weimerskirch et al. 2004), and albatross, terns,
761   and shearwaters in the Southern Indian Ocean (Hyrenbach et al. 2006, Nel et al. 2001). The
762   advent of electronic tagging and telemetry has facilitated investigation of mesoscale niche
763   utilization and behavior by a diverse range of marine animals, including turtles (Gaspar et al.
764   2006, Kobayashi et al. 2011, Polovina et al. 2004), elephant seals (Bailleul et al. 2010,
765   Campagna et al. 2006), shearwaters (Yoda et al. 2014), and penguins (Cotté et al. 2007). In

766 many cases, association of these animals with mesoscale features is directly linked with foraging
767 behavior.
768
769 **8. CONCLUDING REMARKS**
770   Advances in theory, observation, and modeling have facilitated substantial progress in
771 understanding of physical-biological-biogeochemical interactions in the ocean. It has become
772 abundantly clear that the impacts of eddies varies regionally (section 3.7) by virtue of the wealth
773 of processes that contribute (sections 3.1-3.7) and variations in the relative amplitudes at which
774 those mechanisms are expressed. The longstanding debate about the magnitude of the eddy-
775 induced nutrient source in the subtropics continues (section 4.1), whereas potential eddy-driven
776 nutrient sinks have become apparent in subpolar gyres (section 4.2) and in coastal upwelling
777 regions (section 4.3). Appreciation is growing for the role of mesoscale processes in biological
778 dynamics, including eddy-induced Reynolds stresses (section 5), planktonic biodiversity (section
779 6), and niche utilization by higher trophic levels (section 7). Future prospects are bright for
780 further progress in these areas as observational capabilities improve in towed instrumentation
781 (Davis et al. 2005), autonomous platforms (Johnson et al. 2009), genomic methods to
782 characterize planktonic communities (DeLong et al. 2006), and electronic tagging technologies
783 (Block et al. 2001). Increased spatial resolution in upcoming altimeter missions (Fu &
784 Ubelmann 2013) and finer spectral resolution in ocean color missions (Del Castillo 2012) will
785 enhance the abilities to characterize physical and biological properties in the upper ocean.
786 Likewise, computational infrastructure and modeling capabilities continue to progress (Hecht &
787 Hasumi 2008). This confluence of advances in *in situ* observation, remote sensing, and
788 modeling have set the stage to further elucidate the linkages between mesoscale and
789 submesoscale dynamics (Lévy et al. 2012a), which is perhaps one of the most challenging and
790 exciting prospects for future research in this area.
791

796
797
798

799   **References**
800
801   Abraham ER. 1998. The generation of plankton patchiness by turbulent stirring. *Nature* 391:
802   577-80
803   Adams DK, McGillicuddy DJ, Zamudio L, Thurnherr AM, Liang X, et al. 2011. Surface-
804   Generated Mesoscale Eddies Transport Deep-Sea Products from Hydrothermal Vents.
805   *Science* 332: 580-83
806   Alemany F, Quintanilla L, Velez-Belchí P, García A, Cortés D, et al. 2010. Characterization of
807   the spawning habitat of Atlantic bluefin tuna and related species in the Balearic Sea
808   (western Mediterranean). *Progress In Oceanography* 86: 21-38
809   Allen JT, Brown L, Sanders R, Moore CM, Mustard A, et al. 2005. Diatom carbon export
810   enhanced by silicate upwelling in the northeast Atlantic. *Nature* 437: 728-32
811   Altabet MA, Ryabenko E, Stramma L, Wallace DWR, Frank M, et al. 2012. An eddy-stimulated
812   hotspot for fixed nitrogen-loss from the Peru oxygen minimum zone. *Biogeosciences* 9:
813   4897-908
814   Angel MV, Fasham MJR. 1983. Eddies and Biological Processes. In *Eddies in Marine Science*,
815   ed. AR Robinson, pp. 492-524: Springer-Verlag
816   Bailleul F, Cotté C, C G. 2010. Mesoscale eddies as foraging area of a deep-diving predator, the
817   southern elephant seal. *Marine Ecology Progress Series* 408: 251-64
818   Bakun A. 2006. Fronts and eddies as key structures in the habitat of marine fish larvae:
819   opportunity, adaptive response and competitive advantage. *Scientia Marina* 70S2: 105-22
820   Benitez-Nelson CR, Bidigare RR, Dickey TD, Landry MR, Leonard CL, et al. 2007. Mesoscale
821   eddies drive increased silica export in the subtropical Pacific Ocean. *Science* 316: 1017-
822   21
823   Benitez-Nelson CR, McGillicuddy DJ. 2008. Mesoscale physical-biological-biogeochemical
824   linkages in the open ocean: An introduction to the results of the E-FLUX and EDDIES
825   programs. *Deep Sea Res. II* 55: 1133-38
826   Bibby TS, Moore CM. 2011. Silicate:nitrate ratios of upwelled waters control the phytoplankton
827   community sustained by mesoscale eddies in sub-tropical North Atlantic and Pacific.
828   *Biogeosciences* 8: 657-66
829   Bidigare RR, Benitez-Nelson C, Leonard CL, Quay PD, Parsons ML, et al. 2003. Influence of a
830   cyclonic eddy on microheterotroph biomass and carbon export in the lee of Hawaii.
831   *Geophysical Research Letters* 30: 1318
832   Block BA, Dewar H, Blackwell SB, Williams TD, Prince ED, et al. 2001. Migratory
833   Movements, Depth Preferences, and Thermal Biology of Atlantic Bluefin Tuna. *Science*
834   293: 1310-14
835   Bourbonnais A, Altabet MA, Charoenpong CN, Larkum J, Hu H, et al. submitted. N-loss isotope
836   effects in the Peru oxygen minimum zone studied using a mesoscale eddy as a natural
837   tracer experiment. *Global Biogeochemical Cycles*
838   Bracco A, Provenzale A, Scheuring I. 2000. Mesoscale vortices and the paradox of the plankton.
839   *Proceedings of the Royal Society of London B* 267: 1795-800
840   Brentnall SJ, Richards KJ, Brindley J, Murphy E. 2003. Plankton patchiness and its effect on
841   larger-scale productivity. *Journal of Plankton Research* 25: 121-40
842   Broecker WS, Peng TH. 1982. *Tracers in the Sea*. Palisades, New York: Lamont-Doherty
843   Geological Observatory

844   Brzezinski MA, Villareal TA, Lipschultz F. 1998. Silica production and the contribution of
845   diatoms to new and primary production on the central North Pacific. *Marine Ecology -*
846   *Progress Series* 167: 89-104
847   Campagna C, Piola AR, Rosa Marin M, Lewis M, Fernández T. 2006. Southern elephant seal
848   trajectories, fronts and eddies in the Brazil/Malvinas Confluence. *Deep Sea Research I*
849   53: 1907-24
850   Charria G, F. Mélin, I. Dadou, M.-H. Radenac, and V. Garçon. 2003. Rossby wave and ocean
851   color: The cells uplifting hypothesis in the South Atlantic Subtropical Convergence Zone.
852   *Geophys. Res. Lett.* 30: 1125-1-4
853   Chelton DB, Gaube P, Schlax MG, Early JJ, Samelson RM. 2011a. The Influence of Nonlinear
854   Mesoscale Eddies on Near-Surface Oceanic Chlorophyll. *Science* 334: 328-32
855   Chelton DB, Schlax MG. 1996. Global Observations of Oceanic Rossby Waves. *Science* 272:
856   234-38
857   Chelton DB, Schlax MG, Freilich MH, Milliff RF. 2004. Satellite Measurements Reveal
858   Persistent Small-Scale Features in Ocean Winds. *Science* 303: 978-83
859   Chelton DB, Schlax MG, Samelson RM. 2011b. Global observations of nonlinear mesoscale
860   eddies. *Progress In Oceanography* 91: 167-216
861   Chelton DB, Schlax MG, Samelson RM, de Szoeke RA. 2007. Global observations of large
862   oceanic eddies. *Geophys. Res. Lett.* 34: L15606
863   Cipollini P, Cromwell D, Challenor PG, Raffaglio S. 2001. Rossby Waves Detected in Global
864   Ocean Colour Data. *Geophys. Res. Lett.* 28: 323-26
865   Clayton S, Dutkiewicz S, Jahn O, Follows MJ. 2013. Dispersal, eddies, and the diversity of
866   marine phytoplankton. *Limnology and Oceanography: Fluids and Environments* 3: 182-
867   97
868   Clayton S, Nagai T, Follows MJ. 2014. Fine scale phytoplankton community structure across the
869   Kuroshio Front. *Journal of Plankton Research* 36: 1017-30
870   Cotté C, Park Y-H, Guinet C, Bost C-A. 2007. Movements of foraging king penguins through
871   marine mesoscale eddies. *Proceedings of the Royal Society of London B* 274: 2385-91
872   Crawford WR, Brickley PJ, Thomas AC. 2007. Mesoscale eddies dominate surface
873   phytoplankton in northern Gulf of Alaska. *Progress In Oceanography* 75: 287-303
874   d'Ovidio F, De Monte S, Alvain S, Dandonneau Y, Lévy M. 2010. Fluid dynamical niches of
875   phytoplankton types. *Proceedings of the National Academy of Sciences* 107: 18366-70
876   Dandonneau Y, Vega A, Loisel H, Penhoat Yd, Menkes C. 2003. Oceanic Rossby Waves Acting
877   as a "Hay Rake" for Ecosystem Floating By-Products. *Science* 302: 1548-51
878   Davis CS, Thwaites FT, Gallager SM, Hu Q. 2005. A Three-axis Fast-tow Digital Video
879   Plankton Recorder for Rapid Surveys of Plankton Taxa and Hydrography. *Limnology and*
880   *Oceanography: Methods* 3: 59-74
881   Davis RW, Ortega-Ortiz JG, Ribic CA, Evans WE, Biggs DC, et al. 2002. Cetacean habitat in
882   the northern oceanic Gulf of Mexico. *Deep Sea Research I* 49: 121-42
883   Del Castillo C. 2012. *Pre-Aerosol, Clouds, and ocean Ecosystem (PACE) Mission Science*
884   *Definition Team Report*, NASA
885   DeLong EF, Preston CM, Mincer T, Rich V, Hallam SJ, et al. 2006. Community Genomics
886   Among Stratified Microbial Assemblages in the Ocean's Interior. *Science* 311: 496-503
887   Dewar WK. 1986. Mixed layers in Gulf Stream rings. *Dyn. Atmos. Oceans* 10: 1-29
888   Dewar WK, Flierl GR. 1987. Some effects of wind on rings. *Journal of Physical Oceanography*
889   17: 1653-67

890 Dufois F, Hardman-Mountford NJ, Greenwood J, Richardson AJ, Feng M, et al. 2014. Impact of
891   eddies on surface chlorophyll in the South Indian Ocean. *Journal of Geophysical*
892   *Research: Oceans* 119: 8061-77
893 Ebbesmeyer CC, Lindstrom EJ. 1986. Structure and origin of 18C water observed during the
894   POLYMODE Local Dynamics Experiment. *Journal of Physical Oceanography* 16: 443-
895   53
896 Eden C, Dietze H. 2009. Effects of mesoscale eddy/wind interactions on biological new
897   production and eddy kinetic energy. *Journal of Geophysical Research* 114: C05023
898 Falkowski PG, Ziemann D, Kolber Z, Bienfang PK. 1991. Role of eddy pumping in enhancing
899   primary production in the ocean. *Nature* 352: 55-58
900 Flierl GR. 1981. Particle motions in large-amplitude wave fields. *Geophysical & Astrophysical*
901   *Fluid Dynamics* 18: 39-74
902 Flierl GR, McGillicuddy DJ. 2002. Mesoscale and submesoscale physical-biological
903   interactions. In *The Sea*, ed. AR Robinson, JJ McCarthy, BJ Rothschild, pp. 113-85. New
904   York: John Wiley and Sons, Inc.
905 Follows MJ, Dutkiewicz S, Grant S, Chisholm SW. 2007. Emergent biogeography of microbial
906   communities in a model ocean. *Science* 315: 1843–46
907 Franks PJS, Wroblewski JS, Flierl GR. 1986. Prediction of phytoplankton growth in response to
908   the frictional decay of a warm-core ring. *J. Geophys. Res.* 91: 7603-10
909 Fu L-L, Ubelmann C. 2013. On the Transition from Profile Altimeter to Swath Altimeter for
910   Observing Global Ocean Surface Topography. *Journal of Atmospheric and Oceanic*
911   *Technology* 31: 560-68
912 Gaspar P, Georges J-Y, Fossette S, Lenoble A, Ferraroli S, Le Maho Y. 2006. Marine animal
913   behaviour: neglecting ocean currents can lead us up the wrong track. *Proceedings of the*
914   *Royal Society of London B* 273: 2697-702
915 Gaube P, Chelton DB, Samelson RM, Schlax MG, O'Neill LW. 2015. Satellite Observations of
916   Mesoscale Eddy-Induced Ekman Pumping. *Journal of Physical Oceanography* 45: 104-
917   32
918 Gaube P, Chelton DB, Strutton PG, Behrenfeld MJ. 2013. Satellite observations of chlorophyll,
919   phytoplankton biomass and Ekman pumping in nonlinear mesoscale eddies. *Journal of*
920   *Geophysical Research* 118: 6349–70
921 Gaube P, McGillicuddy DJ, Chelton DB, Behrenfeld MJ, Strutton PG. 2014. Regional variations
922   in the influence of mesoscale eddies on near-surface chlorophyll. *Journal of Geophysical*
923   *Research: Oceans* 119: 8195-220
924 Genin A, Jaffe JS, Reef R, Richter C, Franks PJS. 2005. Swimming Against the Flow: A
925   Mechanism of Zooplankton Aggregation. *Science* 308: 860-62
926 Gent PR, Willebrand J, McDougall TJ, McWilliams JC. 1995. Parameterizing Eddy-Induced
927   Tracer Transports in Ocean Circulation Models. *Journal of Physical Oceanography* 25:
928   463-74
929 Godø OR, Samuelsen A, Macaulay GJ, Patel R, Hjøllo SS, et al. 2012. Mesoscale Eddies Are
930   Oases for Higher Trophic Marine Life. *PLoS ONE* 7: e30161
931 Goldman JC. 1988. Spatial and temporal discontinuities of biological processes in pelagic
932   surface waters. In *Toward a Theory on Biological-Physical Interactions in the World*
933   *Ocean*, ed. BJ Rothschild, pp. 273-96. Dordrecht: D. Reidel
934 Goldman JC, McGillicuddy DJ. 2003. Impact of large marine diatoms growing at low light on
935   episodic new production. *Limnol. Oceanogr.* 48: 1176-82

936   Goodman L. 2011. Application of the Robinson biodynamical theory to turbulence. *Dynamics of*
937   *Atmospheres and Oceans* 52: 8-19
938   Goodman L, Robinson AR. 2008. On the theory of advective effects on biological dynamics in
939   the sea. III. The role of turbulence in biological–physical interactions. *Proceedings of the*
940   *Royal Society of London A* 464: 555-72
941   Gower JFR, Denman KL, Holyer RJ. 1980. Phytoplankton patchiness indicates the fluctuation
942   spectrum of mesoscale oceanic structure. *Nature* 288: 157-59
943   Gruber N, Lachkar Z, Frenzel H, Marchesiello P, Munnich M, et al. 2011. Eddy-induced
944   reduction of biological production in eastern boundary upwelling systems. *Nature Geosci*
945   4: 787-92
946   Hecht MW, Hasumi H, eds. 2008. *Ocean Modeling in an Eddying Regime*, Vols. 177.
947   Washington D.C.: American Geophysical Union. 409 pp.
948   Hernández-Carrasco I, Rossi V, Hernández-García E, Garçon V, López C. 2014. The reduction
949   of plankton biomass induced by mesoscale stirring: A modeling study in the Benguela
950   upwelling. *Deep Sea Research I* 83: 65-80
951   Hutchinson GE. 1961. The Paradox of the Plankton. *The American Naturalist* 95: 137-45
952   Hyrenbach KD, Veit RR, Weimerskirch H, Jr. GLH. 2006. Seabird associations with mesoscale
953   eddies: the subtropical Indian Ocean. *Marine Ecology Progress Series* 324: 271-79
954   Jenkins WJ. 1988a. Nitrate flux into the euphotic zone near Bermuda. *Nature* 331: 521-23
955   Jenkins WJ. 1988b. The use of anthropogenic tritium and helium-3 to study subtropical gyre
956   ventilation and circulation. *Phil. Trans. Roy. Soc.* 325: 43-61
957   Jenkins WJ, Goldman J. 1985. Seasonal oxygen cycling and primary production in the Sargasso
958   Sea. *Journal of Marine Research* 43: 465-91
959   Johnson KS, Berelson WM, Boss ES, Chase Z, Claustre H, et al. 2009. Observing
960   biogeochemical cycles at global scales with profiling floats and gliders: Prospects for a
961   global array. *Oceanography* 22: 216-25
962   José YS, Aumont O, Machu E, Penven P, Moloney CL, Maury O. 2014. Influence of mesoscale
963   eddies on biological production in the Mozambique Channel: Several contrasted
964   examples from a coupled ocean-biogeochemistry model. *Deep Sea Research II* 100: 79-
965   93
966   Kahru M, Mitchell BG, Gille ST, Hewes CD, Holm-Hansen O. 2007. Eddies enhance biological
967   production in the Weddell-Scotia Confluence of the Southern Ocean. *Geophysical*
968   *Research Letters* 34: L14603
969   Killworth PD, Cipollini P, Uz BM, Blundell JR. 2004. Physical and biological mechanisms for
970   planetary waves observed in satellite-derived chlorophyll. *J. Geophys. Res.* 109: C07002
971   Klein P, Hua BL. 1988. Mesoscale heterogeneity of the wind-driven mixed layer: Influence of a
972   quasigeostrophic flow. *J. Mar. Res.* 46: 495-525
973   Klein P, Lapeyre G. 2009. The oceanic vertical pump induced by mesoscale and submesoscale
974   turbulence. *Annu. Rev. Mar. Sci.* 2009: 351-75
975   Knauss JA. 1978. *Introduction to Physical Oceanography*. Englewood Cliffs, NJ: Prentice-Hall,
976   Inc. 338 pp.
977   Kobayashi DR, Cheng I-J, Parker DM, Polovina JJ, Kamezaki N, Balazs GH. 2011. Loggerhead
978   turtle (*Caretta caretta*) movement off the coast of Taiwan: characterization of a hotspot
979   in the East China Sea and investigation of mesoscale eddies. *ICES Journal of Marine*
980   *Science: Journal du Conseil* 68: 707-18

Kouketsu S, Tomita H, Oka E, Hosoda S, Kobayashi T, Sato K. 2012. The role of meso-scale eddies in mixed layer deepening and mode water formation in the western North Pacific. *Journal of Oceanography* 68: 63-77

Krause JW, Lomas MW, Nelson DM. 2009. Biogenic silica at the Bermuda Atlantic Time-series Study site in the Sargasso Sea: Temporal changes and their inferred controls based on a 15-year record. *Global Biogeochemical Cycles* 23: GB3004

Krause JW, Nelson DM, Lomas MW. 2010. Production, dissolution, accumulation, and potential export of biogenic silica in a Sargasso Sea mode-water eddy. *Limnology & Oceanography* 55: 569-79

Kunze E. 1985. Near-inertial wave propagation in geostrophic shear. *Journal of Physical Oceanography* 15: 544-656

Lapeyre G, Klein P. 2006. Impact of the small-scale elongated filaments on the oceanic vertical pump. *Journal of Marine Research* 64: 835-51

Lee MM, Williams RG. 2000. The role of eddies in the isopycnic transfer of nutrients and their impact on biological production. *Journal of Marine Research* 58: 895-917

Legendre L, Demers S. 1984. Towards dynamic biological oceanography and limnology. *Can. J. Fish. Aquat. Sci.* 41: 2-19

Lehahn Y, d'Ovidio F, Lévy M, Amitai Y, Heifetz E. 2011. Long range transport of a quasi isolated chlorophyll patch by an Agulhas ring. *Geophysical Research Letters* 38: L16610

Lehahn Y, d'Ovidio F, Lévy M, Heifetz E. 2007. Stirring of the northeast Atlantic spring bloom: A Lagrangian analysis based on multisatellite data. *Journal of Geophysical Research* 112: C08005

Letelier RM, Karl DM, Abbott MR, Flament PJ, Freilich MH, Lukas R. 2000. Role of late winter mesoscale events in the biogeochemical variability of the upper water column of the North Pacific Subtropical Gyre. *J. Geophys. Res.* 105: 28,723-28,39

Lévy M. 2008. The Modulation of Biological Production by Oceanic Mesoscale Turbulence. In *Transport and Mixing in Geophysical Flows*, ed. J Weiss, A Provenzale, pp. 219-61: Springer Berlin Heidelberg

Lévy M, Ferrari R, Franks PJS, Martin AP, Rivière P. 2012a. Bringing physics to life at the submesoscale. *Geophysical Research Letters* 39: L14602

Lévy M, Iovino D, Resplandy L, Klein P, Madec G, et al. 2012b. Large-scale impacts of submesoscale dynamics on phytoplankton: Local and remote effects. *Ocean Modelling* 43-44: 77-93

Lévy M, Jahn O, Dutkiewicz S, Follows MJ. 2014. Phytoplankton diversity and community structure affected by oceanic dispersal and mesoscale turbulence. *Limnology and Oceanography: Fluids and Environments* 4: 67-84

Lévy M, Klein P. 2004. Does the low frequency variability of mesoscale dynamics explain a part of the phytoplankton and zooplankton spectral variability? *Proceedings of the Royal Society of London A: Mathematical, Physical and Engineering Sciences* 460: 1673-87

Lévy M, Klein P, Treguier A-M. 2001. Impact of sub-mesoscale physics on production and subduction of phytoplankton in an oligotrophic regime. *J. Mar. Res.* 59: 535-65

Lévy M, Martin AP. 2013. The influence of mesoscale and submesoscale heterogeneity on ocean biogeochemical reactions. *Global Biogeochemical Cycles* 27: 1139-50

Lévy M, Mémery L, Madec G. 1998. The onset of a bloom after deep winter convection in the northwestern Mediterranean sea: mesoscale process study with a primitive equation model. *Journal of Marine Systems* 16: 7-21

1027 Lévy M, Mémery L, Madec G. 1999. The onset of the Spring Bloom in the MEDOC area:
1028   mesoscale spatial variability. *Deep Sea Research I* 46: 1137-60
1029 Lewis MR. 2002. Variability of Plankton and Plankton Processes on the Mesoscale. In
1030   *Phytoplankton Productivity: Carbon Assimilation in Marine and Freshwater Ecosystems*,
1031   ed. PJlB Williams, DN Thomas, CS Reynolds, pp. 141-55: Blackwell Science Ltd
1032 Li J, Qi Y, Jing Z, Wang J. 2014. Enhancement of eddy-Ekman pumping inside anticyclonic
1033   eddies with wind-parallel extension: Satellite observations and numerical studies in the
1034   South China Sea. *Journal of Marine Systems* 132: 150-61
1035 Lima ID, Olson DB, Doney SC. 2002. Biological response to frontal dynamics and mesoscale
1036   variability in oligotrophic environments: Biological production and community structure.
1037   *Journal of Geophysical Research: Oceans* 107: 25-1-25-21
1038 Lindo-Atichati D, F. B, G. G, B. M, Muller-Karger FE, Habtes S. 2012. Varying mesoscale
1039   structures influence larval fish distribution in the northern Gulf of Mexico. *Marine
1040   Ecology Progress Series* 463: 245-57
1041 Lobel PS, Robinson AR. 1986. Transport and entrapment of fish larvae by ocean mesoscale
1042   eddies and currents in Hawaiian waters. *Deep-Sea Research* 33: 483-500
1043 Mackas DL, Denman KL, Abbott MR. 1985. Plankton patchiness: biology in the physical
1044   vernacular. *Bull. Mar. Sci.* 37: 652-74
1045 Mahadevan A. 2016. Impact of Submesoscale Physics on Primary Productivity of Plankton.
1046   *Annual Review of Marine Science* 8: null
1047 Mahadevan A, D'Asaro E, Lee C, Perry MJ. 2012. Eddy-Driven Stratification Initiates North
1048   Atlantic Spring Phytoplankton Blooms. *Science* 337: 54-58
1049 Mahadevan A, Thomas LN, Tandon A. 2008. Comment on "Eddy/Wind Interactions Stimulate
1050   Extraordinary Mid-Ocean Plankton Blooms". *Science* 320: DOI:
1051   10.1126/science.1152111
1052 Marshall D. 1997. Subduction of water masses in an eddying ocean. *Journal of Marine Research*
1053   55: 201– 22
1054 Martin AP. 2003. Phytoplankton patchiness: the role of lateral stirring and mixing. *Progress In
1055   Oceanography* 57: 125-74
1056 Martin AP, Lévy M, van Gennip S, Pardo S, Srokosz M, et al. submitted. An observational
1057   assessment of the influence of mesoscale and submesoscale heterogeneity on ocean
1058   biogeochemical reactions. *Global Biogeochemical Cycles*
1059 Martin AP, Pondaven P. 2003. On estimates for the vertical nitrate flux due to eddy pumping.
1060   *Journal of Geophysical Research: Oceans* 108: 3359
1061 Martin AP, Richards KJ. 2001. Mechanisms for vertical nutrient transport within a North
1062   Atlantic mesoscale eddy. *Deep-Sea Research II* 48: 757-73
1063 Martin AP, Richards KJ, Law CS, Liddicoat M. 2001. Horizontal dispersion within an
1064   anticyclonic mesoscale eddy. *Deep Sea Research II* 48: 739-55
1065 McGillicuddy DJ. 2011. Eddies Masquerade as Planetary Waves. *Science* 334: 318-19
1066 McGillicuddy DJ. 2015. Formation of Intra-thermocline Lenses by Eddy-wind Interaction.
1067   *Journal of Physical Oceanography* 45: 606-12
1068 McGillicuddy DJ, Anderson LA, Bates NR, Bibby T, Buesseler KO, et al. 2007. Eddy/wind
1069   interactions stimulate extraordinary mid-ocean plankton blooms. *Science* 316: 1021-26
1070 McGillicuddy DJ, Anderson LA, Doney SC, Maltrud ME. 2003. Eddy-driven sources and sinks
1071   of nutrients in the upper ocean: Results from a 0.1° resolution model of the North
1072   Atlantic. *Global Biogeochemical Cycles* 17: 1035 doi:10.29/2002GB001987

1073 McGillicuddy DJ, Robinson A, Siegel D, Jannasch HW, Johnson R, et al. 1998. Influence of
1074   mesoscale eddies on new production in the Sargasso Sea. *Nature* 394: 263-65
1075 McGillicuddy DJ, Robinson AR. 1997. Eddy induced nutrient supply and new production in the
1076   Sargasso Sea. *Deep-Sea Research I* 44: 1427-49
1077 McGillicuddy DJ, Robinson AR, McCarthy JJ. 1995. Coupled physical and biological modeling
1078   of the spring bloom in the North Atlantic: (II) Three dimensional bloom and post-bloom
1079   effects. *Deep-Sea Research* 42: 1359-98
1080 McNeil JD, Jannasch HW, Dickey TD, McGillicuddy DJ, Brzezinski M, Sakamoto CM. 1999.
1081   New chemical, bio-optical and physical observations of upper ocean response to the
1082   passage of a mesoscale eddy off Bermuda. *J. Geophys. Res.* 104: 15537-48
1083 McWilliams JC. 2008. The Nature and Consequences of Oceanic Eddies. In *Ocean Modeling in
1084   an Eddying Regime*, pp. 5-15: American Geophysical Union
1085 Mémery L, Reverdin G, Paillet J, Oschlies A. 2005. Introduction to the POMME special section:
1086   Thermocline ventilation and biogeochemical tracer distribution in the northeast Atlantic
1087   Ocean and impact of mesoscale dynamics. *Journal of Geophysical Research: Oceans*
1088   110: C07S01
1089 Menkes CE, Kennan SC, Flament P, Dandonneau Y, Masson S, et al. 2002. A whirling
1090   ecosystem in the equatorial Atlantic. *Geophysical Research Letters* 29: 1-4
1091 Miller LA, Robert M, Crawford WR. 2005. The large, westward-propagating Haida Eddies of
1092   the Pacific eastern boundary. *Deep Sea Research II* 52: 845-51
1093 Mitarai S, Siegel DA, Watson JR, Dong C, McWilliams JC. 2009. Quantifying connectivity in
1094   the coastal ocean with application to the Southern California Bight. *Journal of
1095   Geophysical Research: Oceans* 114: C10026
1096 Mizobata K, Saitoh SI, Shiomoto A, Miyamura T, Shiga N, et al. 2002. Bering Sea cyclonic and
1097   anticyclonic eddies observed during summer 2000 and 2001. *Progress In Oceanography*
1098   55: 65-75
1099 Moore TS, Matear RJ, Marra J, Clementson L. 2007. Phytoplankton variability off the Western
1100   Australian Coast: Mesoscale eddies and their role in cross-shelf exchange. *Deep Sea
1101   Research II* 54: 943-60
1102 Nel DC, Lutjeharms JRE, Pakhomov EA, Ansorge IJ, Ryan PG, Klages NTW. 2001.
1103   Exploitation of mesoscale oceanographic features by grey-headed albatross Thalassarche
1104   chrysostoma in the southern Indian Ocean. *Marine Ecology Progress Series* 217: 15-26
1105 Nelepo BA, ed. 1983. *Experimental investigations under the international POLYMODE
1106   program*. New Delhi: Oxonian Press. 143 pp.
1107 Nelson DM, McCarthy JJ, Joyce TM, Ducklow HW. 1989. Enhanced near-surface nutrient
1108   availability and new production resulting from the frictional decay of a Gulf\0Stream
1109   warm-core ring. *Deep-Sea Research* 36: 705-14
1110 Niiler PP. 1969. On the Ekman divergence in an oceanic jet. *Journal of Geophysical Research*
1111   74: 7048-52
1112 Nurser AJG, Zhang JW. 2000. Eddy-induced mixed layer shallowing and mixed
1113   layer/thermocline exchange. *Journal of Geophysical Research: Oceans* 105: 21851-68
1114 Olaizola M, Ziemann DA, Bienfang PK, Walsh WA, Conquest LD. 1993. Eddy-induced
1115   oscillations of the pycnocline affect the floristic composition and depth distribution of
1116   phytoplankton in the subtropical Pacific. *Marine Biology* V116: 533-42
1117 Olson DB, Backus RH. 1985. The concentrating of organisms at fronts: A cold-water fish and a
1118   warm-core Gulf Stream ring. *J. Mar. Res.* 43: 113-37

1119 Oschlies A. 2002. Can eddies make ocean deserts bloom? *Global Biogeochem. Cycles* 16: 1106
1120 Oschlies A. 2008. Eddies and Upper-Ocean Nutrient Supply. In *Ocean Modeling in an Eddying*
1121   *Regime*, pp. 115-30: American Geophysical Union
1122 Oschlies A, Garcon VC. 1998. Eddy-induced enhancement of primary production in a model of
1123   the North Atlantic Ocean. *Nature* 394: 266-69
1124 Pascual A, Faugère Y, Larnicol G, LeTraon PY. 2006. Improved description of the ocean
1125   mesoscale variability by combining four satellite altimeters. *Geophys. Res. Lett.* 33:
1126   L02611
1127 Pasquero C, Bracco A, Provenzale A. 2005. Impact of the spatiotemporal variability of the
1128   nutrient flux on primary productivity in the ocean. *Journal of Geophysical Research:*
1129   *Oceans* 110: C07005
1130 Pearce AF, Griffiths RW. 1991. The mesoscale structure of the Leeuwin Current: A comparison
1131   of laboratory models and satellite imagery. *Journal of Geophysical Research: Oceans* 96:
1132   16739-57
1133 Perruche C, Rivière P, Lapeyre G, Carton X, Pondaven P. 2011. Effects of surface quasi-
1134   geostrophic turbulence on phytoplankton competition and coexistence. *Journal of Marine*
1135   *Research* 69: 105-35
1136 Pingree RD, Holligan PM, Mardell GT. 1979. Phytoplankton growth and cyclonic eddies. *Nature*
1137   278: 245-47
1138 Polovina JJ, Balazs GH, Howell EA, Parker DM, Seki MP, Dutton PH. 2004. Forage and
1139   migration habitat of loggerhead (*Caretta caretta*) and olive ridley (*Lepidochelys*
1140   *olivacea*) sea turtles in the central North Pacific Ocean. *Fisheries Oceanography* 13: 36-
1141   51
1142 Prasanna Kumar S, Nuncio M, Ramaiah N, Sardesai S, Narvekar J, et al. 2007. Eddy-mediated
1143   biological productivity in the Bay of Bengal during fall and spring intermonsoons. *Deep*
1144   *Sea Research I* 54: 1619-40
1145 Provenzale A. 1999. Transport by coherent barotropic vortices. *Annual Review of Fluid*
1146   *Mechanics* 31: 55-93
1147 Radchenko LA. 1983. Quantitative distribution of seston in the region. In *Experimental*
1148   *investigations under the international POLYMODE program*, ed. BA Nelepo, pp. 129-35.
1149   New Delhi: Oxonian Press
1150 Resplandy L, Lévy M, Madec G, Pous S, Aumont O, Kumar D. 2011. Contribution of mesoscale
1151   processes to nutrient budgets in the Arabian Sea. *Journal of Geophysical Research:*
1152   *Oceans* 116: C11007
1153 Richardson DE, Llopiz JK, Guigand CM, Cowen RK. 2010. Larval assemblages of large and
1154   medium-sized pelagic species in the Straits of Florida. *Progress In Oceanography* 86: 8-
1155   20
1156 Ring Group. 1981. Gulf Stream cold-core rings: their physics, chemistry and biology. *Science*
1157   212: 1091-100
1158 Rodriguez J, Tintore J, Allen JT, Blanco JM, Gomis D, et al. 2001. Mesoscale vertical motion
1159   and the size structure of phytoplankton in the ocean. *Nature* 410: 360-63
1160 Rossi V, López C, Sudre J, Hernández-García E, Garçon V. 2008. Comparative study of mixing
1161   and biological activity of the Benguela and Canary upwelling systems. *Geophysical*
1162   *Research Letters* 35: L11602

1163   Roukhiyainen MI, Yunev OA. 1983. Phytoplankton and primary productin in the wester
1164   Sargasso Sea in summer 1977. In *Experimental investigations under the international*
1165   *POLYMODE program*, ed. BA Nelepo, pp. 120-28. New Delhi: Oxonian Press
1166   Savidge G, Williams PJlB. 2001. The PRIME 1996 cruise: an overview. *Deep-Sea Research II*
1167   48: 687-704
1168   Seki MP, Lumpkin R, Flament P. 2002. Hawaii Cyclonic Eddies and Blue Marlin Catches: The
1169   Case Study of the 1995 Hawaiian International Billfish Tournament. *Journal of*
1170   *Oceanography* 58: 739-45
1171   Seki MP, Polovina JJ, Brainard RE, Bidigare RR, Leonard CL, Foley DG. 2001. Biological
1172   enhancement at cyclonic eddies tracked with GOES Thermal Imagery in Hawaiian
1173   waters. *Geophysical Research Letters* 28: 1583-86
1174   Shulenberger E, Reid JL. 1981. The Pacific shallow oxygen maximum, deep chlorophyll
1175   maximum, and primary productivity, reconsidered. *Deep-Sea Res.* 28A: 901-19
1176   Siegel DA, Court DB, Menzies DW, Peterson P, Maritorena S, Nelson NB. 2008. Satellite and in
1177   situ observations of the bio-optical signatures of two mesoscale eddies in the Sargasso
1178   Sea. *Deep-Sea Research II* 55: 1218-30
1179   Siegel DA, Peterson P, McGillicuddy DJ, Jr., Maritorena S, Nelson NB. 2011. Bio-optical
1180   footprints created by mesoscale eddies in the Sargasso Sea. *Geophys. Res. Lett.* 38:
1181   L13608
1182   Srokosz MA, Martin AP, Fasham MJR. 2003. On the role of biological dynamics in plankton
1183   patchiness at the mesoscale: An example from the eastern North Atlantic Ocean. *Journal*
1184   *of Marine Research* 61: 517-37
1185   Stern ME. 1965. Interaction of a uniform wind stress with a geostrophic vortex. *Deep-Sea*
1186   *Research* 12: 355-67
1187   Stramma L, Bange HW, Czeschel R, Lorenzo A, Frank M. 2013. On the role of mesoscale eddies
1188   for the biological productivity and biogeochemistry in the eastern tropical Pacific Ocean
1189   off Peru. *Biogeosciences* 10: 7293-306
1190   Strass VH. 1992. Chlorophyll patchiness caused by mesoscale upwelling at fronts. *Deep-Sea*
1191   *Res.* 39: 75-96
1192   Sweeney EN, McGillicuddy DJ, Buesseler KO. 2003. Biogeochemical impacts due to mesoscale
1193   eddy activity in the Sargasso Sea as measured at the Bermuda Atlantic Time Series
1194   (BATS) site. *Deep-Sea Res. II* 50: 3017-39
1195   Teo SLH, Block BA. 2010. Comparative Influence of Ocean Conditions on Yellowfin and
1196   Atlantic Bluefin Tuna Catch from Longlines in the Gulf of Mexico. *PLoS ONE* 5: e10756
1197   Ternon JF, Bach P, Barlow R, Huggett J, Jaquemet S, et al. 2014. The Mozambique Channel:
1198   From physics to upper trophic levels. *Deep Sea Research II* 100: 1-9
1199   Tew Kai E, Marsac F. 2010. Influence of mesoscale eddies on spatial structuring of top
1200   predators' communities in the Mozambique Channel. *Progress In Oceanography* 86:
1201   214-23
1202   Uz BM, Yoder JA, Osychny V. 2001. Pumping of nutrients to ocean surface waters by the action
1203   of propagating planetary waves. *Nature* 409: 597-600
1204   Vaillancourt RD, Marra J, Seki MP, Parsons ML, Bidigare RR. 2003. Impact of a cyclonic eddy
1205   on phytoplankton community structure and photosynthetic competency in the subtropical
1206   North Pacific Ocean. *Deep Sea Research I* 50: 829-47
1207   Venrick EL. 1990. Mesoscale patterns of chlorophyll *a* in the central North Pacific. *Deep-Sea*
1208   *Research* 37: 1017-31

1209 Waite AM, Thompson PA, Pesant S, Feng M, Beckley LE, et al. 2007. The Leeuwin Current and
1210   its eddies: An introductory overview. *Deep Sea Research II* 54: 789-96
1211 Wallhead PJ, Garçon VC, Martin AP. 2013. Efficient upscaling of ocean biogeochemistry.
1212   *Ocean Modelling* 63: 40-55
1213 Wallhead PJ, Martin AP, Srokosz MA. 2008. Spatially implicit plankton population models:
1214   transient spatial variability. *Journal of Theoretical Biology* 253: 405-23
1215 Warm Core Rings Executive Committee. 1982. Multidisciplinary program to study warm core
1216   rings. *Eos, Transactions American Geophysical Union* 63: 834-35
1217 Weimerskirch H, Corre ML, Jaquemet Sb, Potier M, Marsac F. 2004. Foraging strategy of a top
1218   predator in tropical waters: great frigatebirds in the Mozambique Channel. *Marine*
1219   *Ecology Progress Series* 275: 297-308
1220 Wiebe PH, Flierl GR. 1983. Euphausiid invasion / dispersal in Gulf Stream cold-core rings.
1221   *Australian Journal of Marine and Freshwater Research* 34: 625-52
1222 Wiebe PH, Joyce TM. 1992. Introduction to interdisciplinary studies of Kuroshio and Gulf
1223   Stream Rings. *Deep-Sea Research* 39: S1-S6
1224 Wiebe PH, McDougall TJ. 1986. Introduction to a collection of papers on warm-core rings. *Deep*
1225   *Sea Research* 33: 1455-57
1226 Williams RG. 1988. Modification of ocean eddies by air-sea interaction. *Journal of Geophysical*
1227   *Research: Oceans* 93: 15523-33
1228 Williams RG, Follows MJ. 1998. The Ekman transfer of nutrients and maintenance of new
1229   production over the North Atlantic. *Deep-Sea Research I* 45: 461-89
1230 Williams RG, Follows MJ. 2003. Physical transport of nutrients and the maintenance of
1231   biological production. In *Ocean Biogeochemistry: The Role of the Ocean Carbon Cycle*
1232   *in Global Change*, ed. MJR Fasham, pp. 19-51. Berlin: Springer-Verlag
1233 Williams RG, Follows MJ. 2011. *Ocean dynamics and the carbon cycle: principles and*
1234   *mechanisms*. Cambridge, UK: Cambridge University Press. 404 pp.
1235 Woods JD. 1988. Mesoscale upwelling and primary production. In *Toward a Theory on*
1236   *Biological-Physical Interactions in the World Ocean*, ed. BJ Rothschild, pp. 7-23.
1237   Dordrecht: D. Reidel
1238 Xiu P, Chai F. 2011. Modeled biogeochemical responses to mesoscale eddies in the South China
1239   Sea. *Journal of Geophysical Research: Oceans* 116: C10006
1240 Xiu P, Palacz AP, Chai F, Roy EG, Wells ML. 2011. Iron flux induced by Haida eddies in the
1241   Gulf of Alaska. *Geophysical Research Letters* 38: L13607
1242 Yoda K, Shiomi K, Sato K. 2014. Foraging spots of streaked shearwaters in relation to ocean
1243   surface currents as identified using their drift movements. *Progress In Oceanography*
1244   122: 54-64
1245 Yoshimori A, Kishi MJ. 1994. Effects of interaction between two warm-core rings on
1246   phytoplankton distribution. *Deep Sea Research I* 41: 1039-52
1247 Zhou K, Dai M, Kao S-J, Wang L, Xiu P, et al. 2013. Apparent enhancement of 234Th-based
1248   particle export associated with anticyclonic eddies. *Earth and Planetary Science Letters*
1249   381: 198-209
1250
1251
1252

1253
1254

| Eddy type	MLD anomaly	CHL anomaly	
		Nutrient limited	Light limited
Cyclone	-	-	+
Anticyclone	+	+	-

1255
1256 **Table 1.** Upper ocean chlorophyll (CHL) anomalies expected from anomalies in mixed layer
1257 depth (MLD) associated with cyclones and anticyclones in different regimes limited by nutrients
1258 and light. Note this idealized summary does not represent mode-water eddies, which constitute a
1259 special case of anticyclones.

1260
1261
1262

Program	Area	Reference
POLYMODE	Sargasso Sea	Nelepo (1983)
Cold Core Rings	Gulf Stream	Ring Group (1981)
Warm Core Rings	Gulf Stream, Kuroshio, East Australia Current	Wiebe & McDougall (1986) Wiebe and Joyce (1992)
PRIME	Northeast Atlantic	Savidge & Williams (2001)
POMME	Northeast Atlantic	Mémery et al. (2005)
Haida Eddy Project	Gulf of Alaska	Miller et al. (2005)
Eddies 2003	Leeuwin Current	Waite et al. (2007)
E-FLUX	Hawaiian lee eddies	Benitez-Nelson & McGillicuddy (2008)
EDDIES	Sargasso Sea	Benitez-Nelson & McGillicuddy (2008)
MESOBIO	Mozambique Channel	Ternon (2014)

1263
1264 **Supplementary Table**. Interdisciplinary *in situ* process studies of mesoscale eddies. Please
1265 forward information on additional studies that should be included to dmcgillicuddy@whoi.edu
1266 so that the living document located at
1267 http://science.whoi.edu/users/mcgillic/eddy_process_studies/table.pdf can be made more
1268 complete and kept current.
1269

1270

Number Cyclonic=18469   Number Anticyclonic=17422
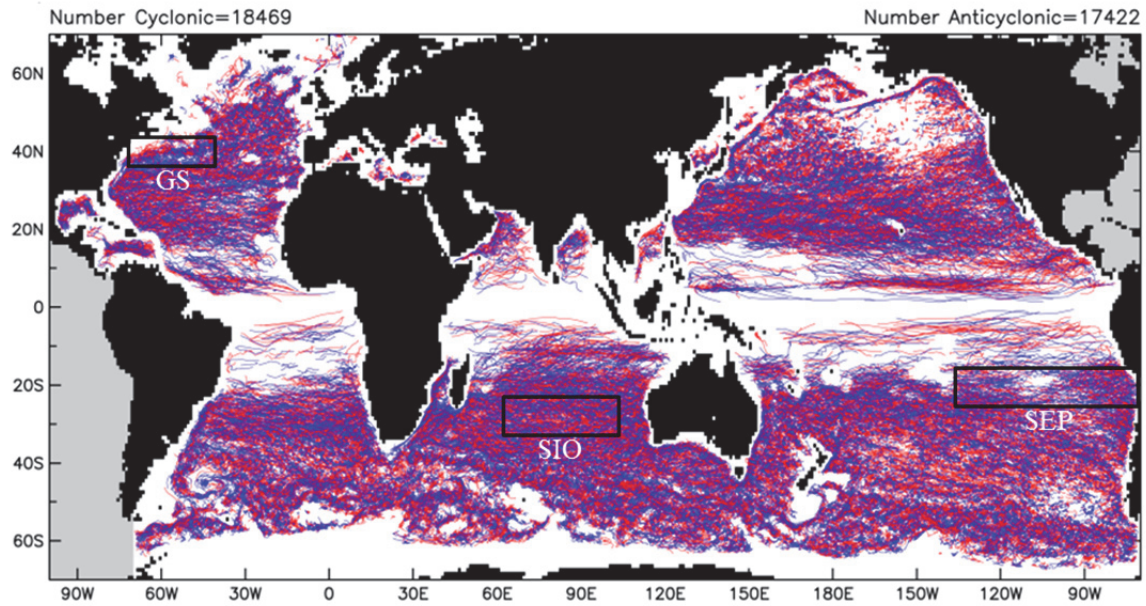
1271
1272
1273 **Figure 1.** Tracks of long-lived (lifetimes ≥ 16 weeks) mesoscale eddies identified by an
1274 automated eddy tracking procedure (Chelton et al. 2011b). Red tracks represent anticyclones
1275 and blue tracks cyclones. Three regional subdomains are indicated: Southeast Pacific (SEP), the
1276 Gulf Stream region (GS), and South Indian Ocean (SIO). Figure adapted from Chelton et al.
1277 (2011b), courtesy of Peter Gaube.
1278
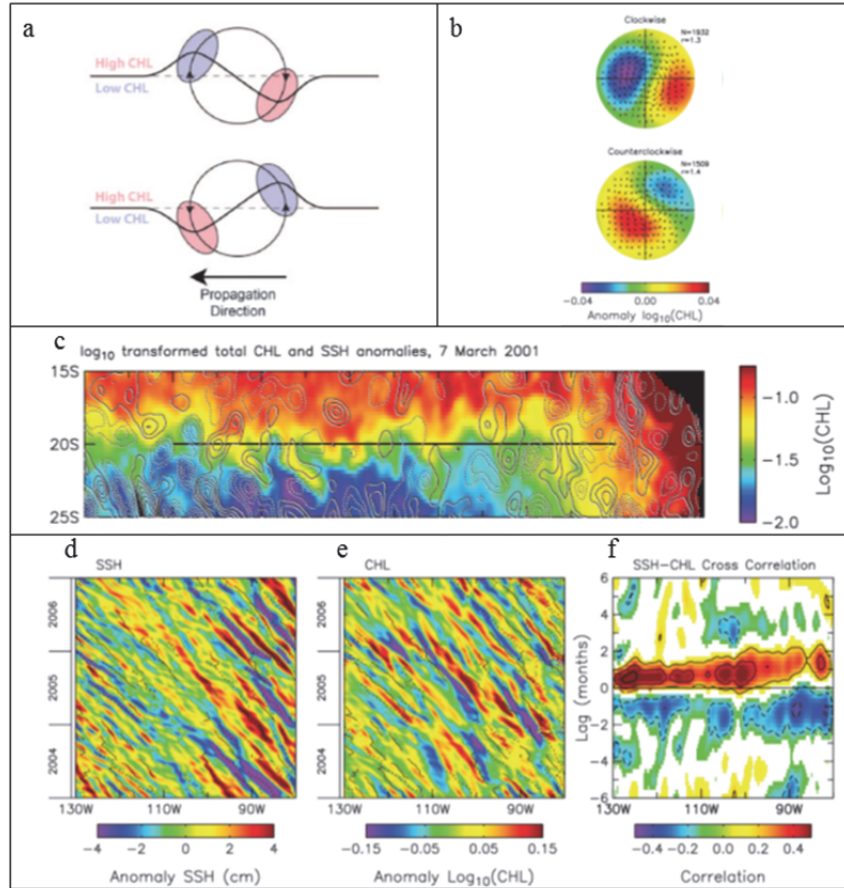
Figure 2. (a) Schematic diagram of eddy-driven stirring of CHL for clockwise (top) and counter-clockwise (bottom) rotating eddies propagating westward in regions where the CHL gradient is northward. An otherwise smooth contour of CHL (dashed lines) is distorted by the rotational velocity field within the eddy, as shown by the solid lines. Advection of CHL within the large-scale background CHL gradient results in the positive and negative CHL anomalies shown by the red and purple regions, respectively. (b) Composite averages for clockwise (top) and counter-clockwise (bottom) eddies in the region labeled "SEP" in **Figure 1**. The outer perimeter of each circle corresponds to twice the eddy radius scale. The vectors in each panel are the gradient of the composite average SSH, which is proportional to the geostrophic velocity. The number N of eddy realizations in the composite average and the magnitude r of the ratio of the primary pole in the leading (left) half of each composite to the secondary pole in the trailing (right) half are labeled on each panel. (c) An example map from the SEP region for 7 March 2001 showing $\log_{10}$(CHL) in color with contours of positive and negative anomaly SSH (solid and dashed lines, respectively) at intervals of 2 cm, excluding the zero contour. The horizontal line indicates the section along which the time-longitude plots in panels d and e are presented. (d) SSH with eddy tracks within ±2°of 20°S overlaid (dashed and solid lines for CW and CC rotating eddies, respectively); (e) log10(CHL) with the same eddy tracks overlaid. (f) Lagged cross-correlation between $\log_{10}$(CHL) at time t and SSH at time t + lag, calculated over the full 10-year data record; the white areas correspond to correlations smaller than the estimated 95% significance level. Positive lags correspond to $\log_{10}$(CHL) leading SSH, and the contour interval is 0.2 with the zero contour omitted for clarity. From Chelton et al. (2011a).
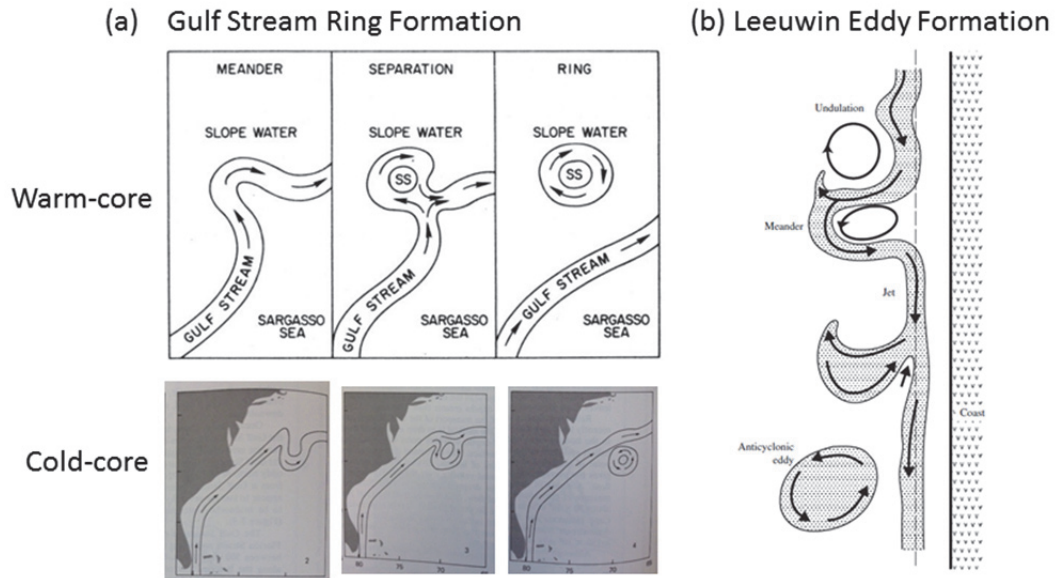
Figure 3. Processes of (a) Gulf Stream Ring formation, and (b) anticyclone generation in the Leeuwin current. Panel (a): (top) adapted from The Warm Core Rings Executive Committee (1982), bottom adapted from Knauss (1978); panel (b) adapted from Moore et al. (2007) and Pearce and Griffiths (1991).
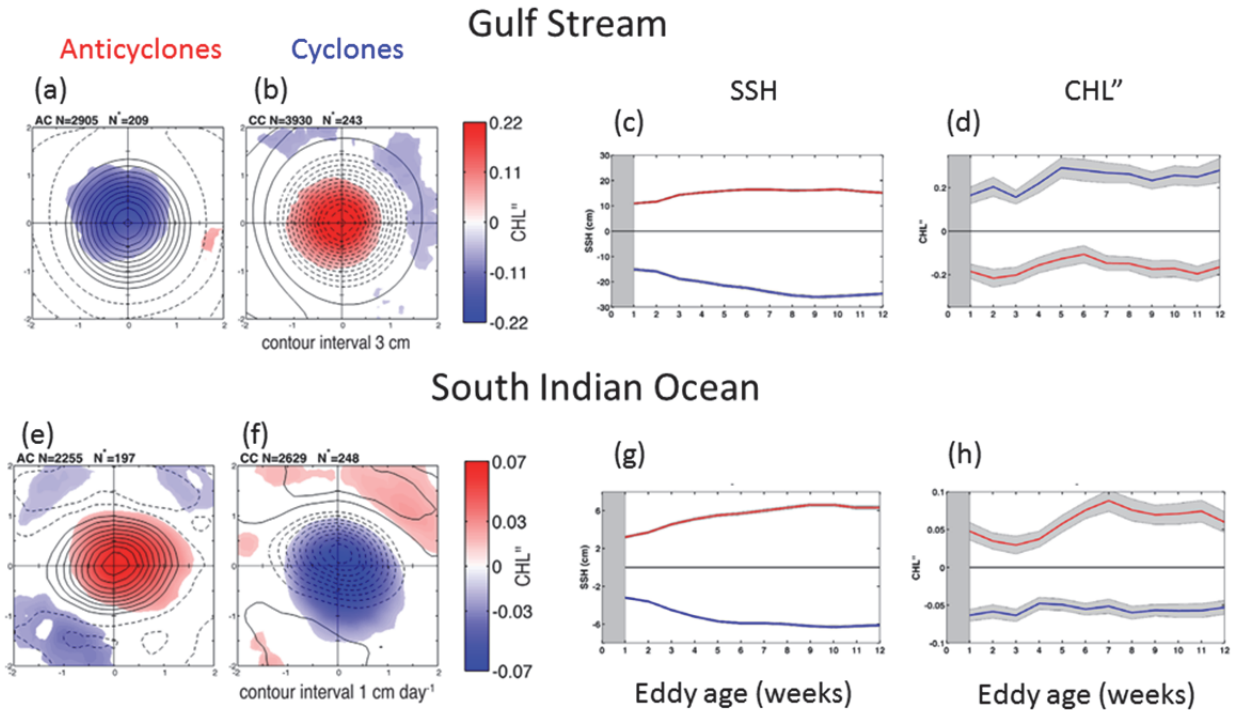
Figure 4. Composite averages of eddy-centric CHL anomaly in (a,b) the Gulf Stream region (year round), and (e,f) the South Indian Ocean (May-October). Locations of the two domains are shown in **Figure 1**. Contours in panels (a) and (b) are SSH anomaly, and eddy-induced Ekman pumping in panels (e) and (f). Regions of the composites that do not exceed the 95% confidence interval of mean are masked with white. The x and y coordinates of the composite averages are normalized by the eddy radius. The title of each composite average indicates both the number of eddy realizations N used to construct the composite and the effective degrees of freedom N^* used to computed the 95% confidence interval. Right hand panels depict time-series of eddy amplitude and CHL anomaly for cyclones (blue) and anticyclones (red). The beginning of the time series are shaded to indicate that both eddy amplitude and CHL anomaly are only observed after the eddy is first detected by the automated eddy tracking procedure, defined here as week 1. From Gaube et al. (2014).

34
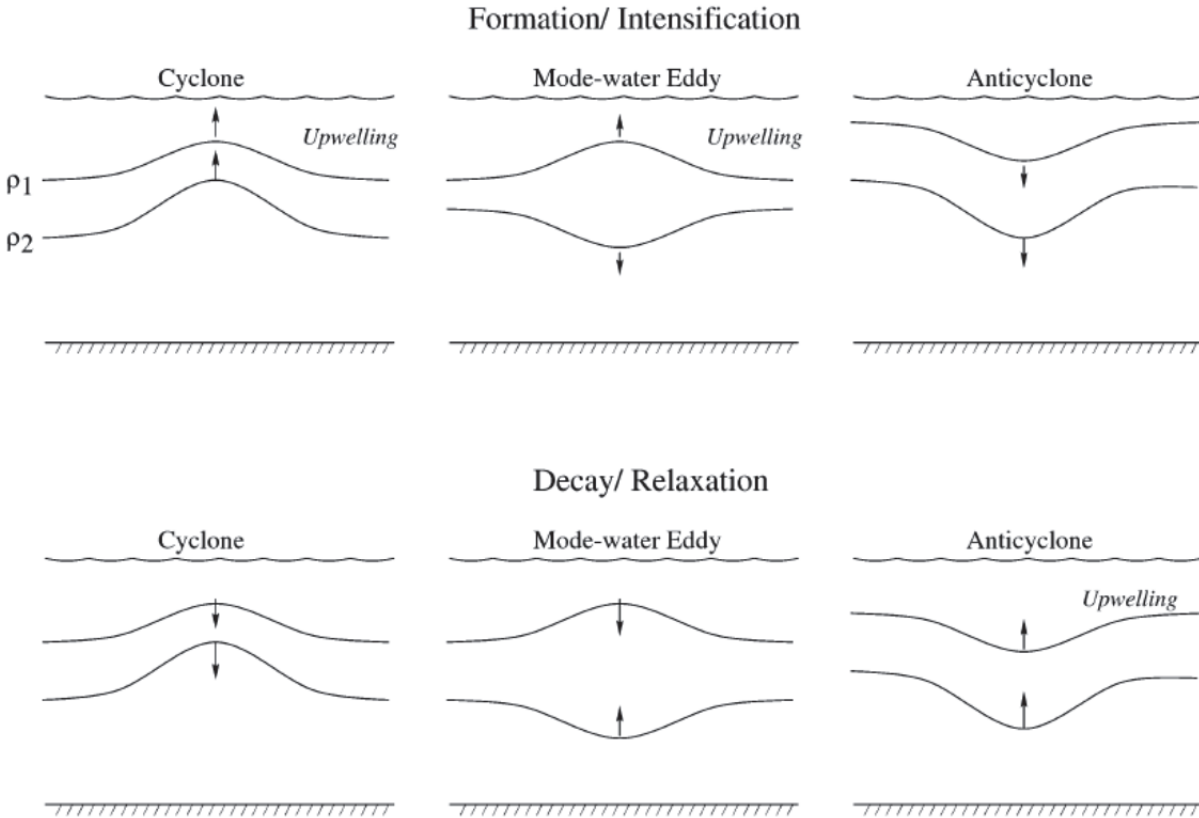
Figure 5. Isopycnal displacements associated with three types of eddies in the process of formation/intensification (top row) and decay (bottom row). Two density surfaces are depicted in each case: one in the seasonal thermocline (ρ_1) and one in the main thermocline (ρ_2). From Flierl and McGillicuddy (2002).
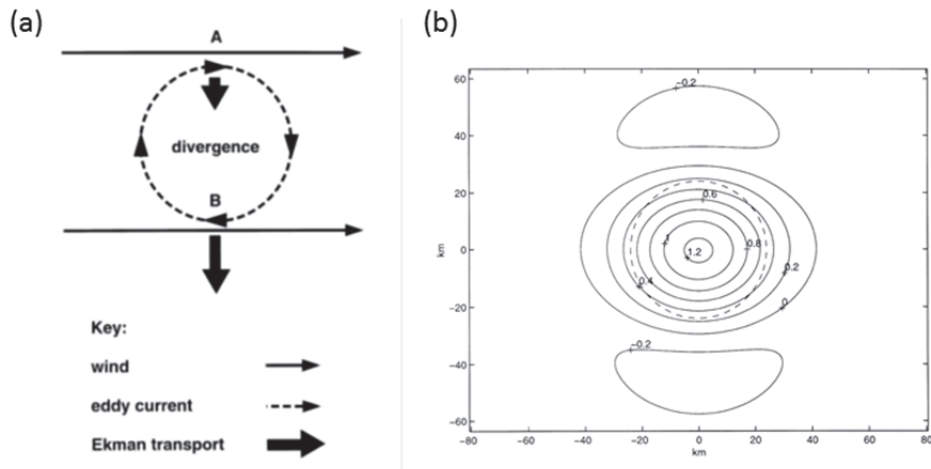
1334
1335
1336 **Figure 6.** (a) Illustration of how a uniform wind applied to an anticyclonic eddy can lead to a
1337 divergence and upwelling in the eddy interior. The surface current reduces the stress where the
1338 wind is in the same direction as the current (point A), and increases it where the wind and current
1339 oppose each other (point B). The difference in the magnitude of the associated Ekman transport
1340 creates a divergence at eddy center, regardless of the direction of the wind. (b) Vertical velocity
1341 field at the base of the Ekman layer for an idealized circular eddy subject to a 15 m s^{-1} wind.
1342 Contour intervals are 0.2 m d^{-1} with positive values denoting upwelling. The dotted line
1343 corresponds to the radius at which the maximum azimuthal velocity occurs. From Martin and
1344 Richards (2001).
1345
1346
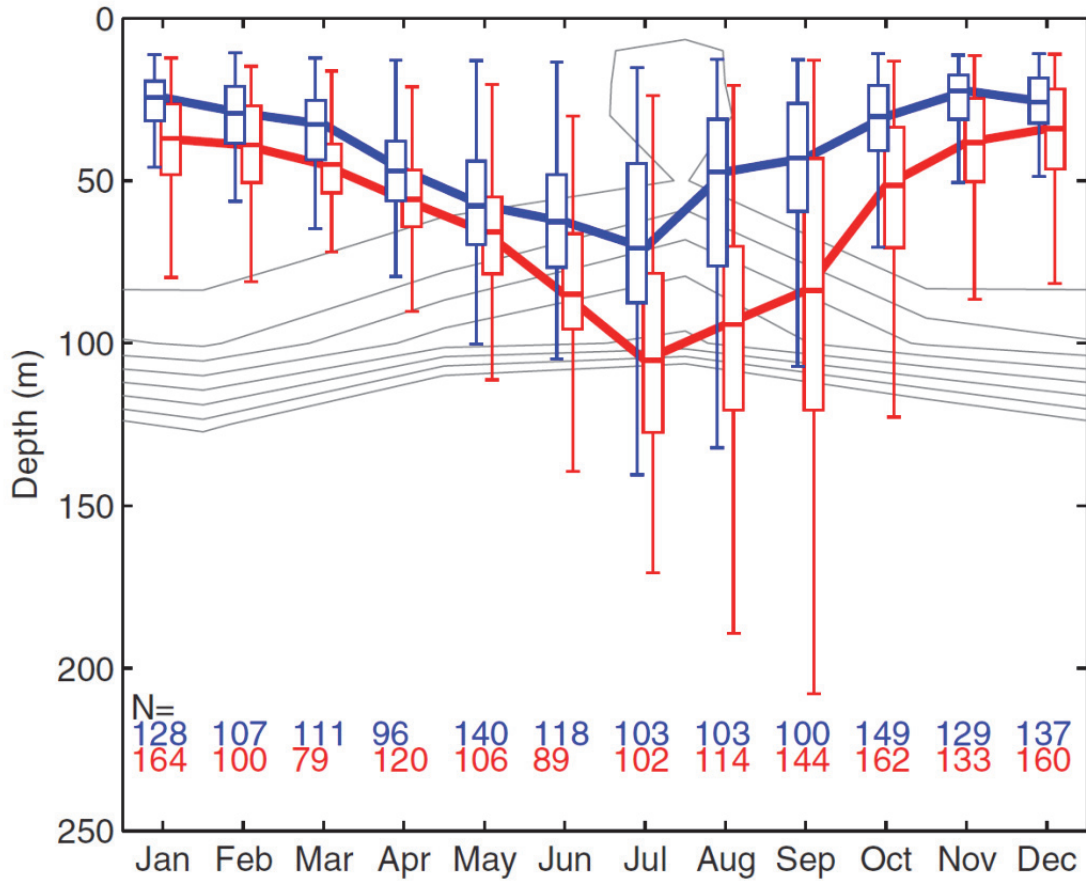
Figure 7. Climatological average mixed layer depths in cyclonic (blue) and anticyclonic (red) eddy interiors from ARGO floats in the South Indian Ocean (region similar to "SIO" in Figure 1). The number N of ARGO floats used for each month is reported. The thin gray lines correspond to the NO_3 mean seasonal contours (from World Ocean Atlas 2009) ranging from 0.3 to 1 mmol m^{-3}. For each time point, the rectangular box is delimited by the lower quartile (Q1) and the upper quartile (Q3), while the median is represented inside the box by a straight line. Whiskers are drawn to the extreme values that are inside the fences lying at Q1-1.5 X (Q3–Q1) and Q3+1.5 X (Q3–Q1). Lines join median values. From Dufois et al. (2014).
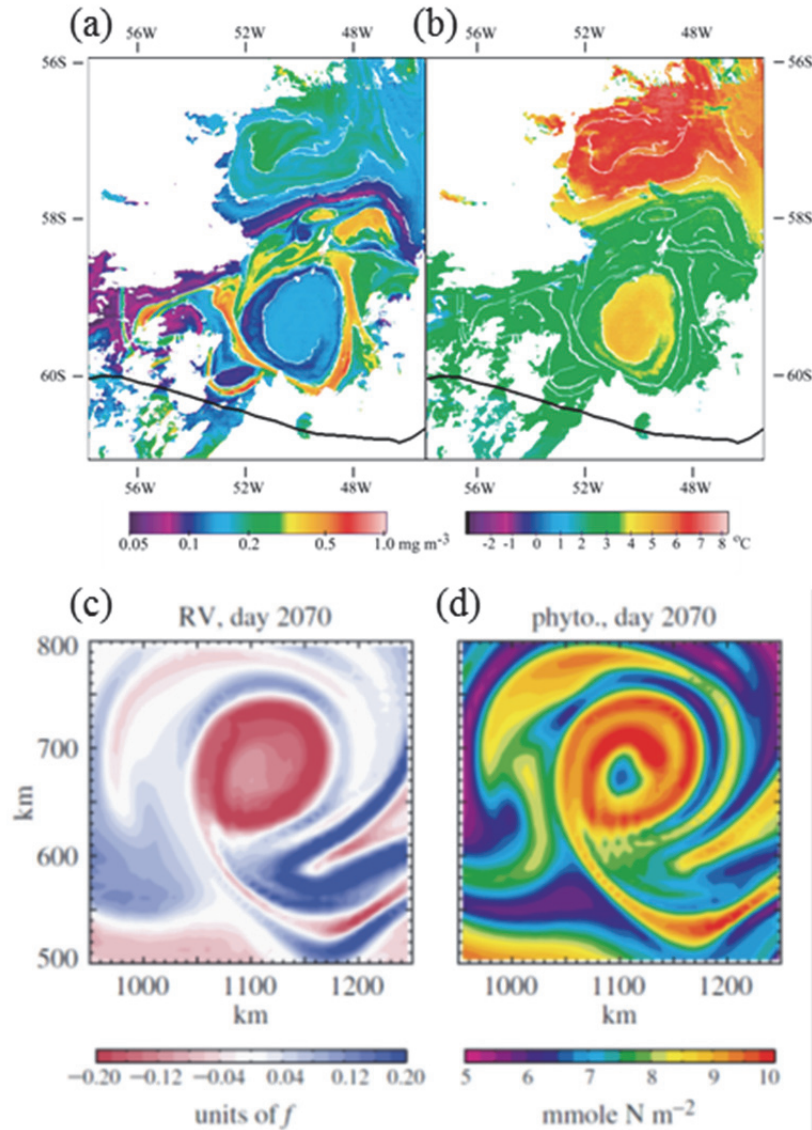
Figure 8. A large anticyclonic eddy north of the mean position of the Southern Antarctic Circumpolar Current front (black curve) on Jan 28, 2004: (a) CHL and (b) sea surface temperature. Ocean areas covered by clouds are shown in white. The white curves are edges determined on the CHL image but overlaid on both images. Lower panels show output from a numerical model highlighting an anticyclonic eddy. Negative relative vorticity in panel (c) is accompanied by high phytoplankton concentration around the periphery of the vortex (d). Note that the sense of rotation is clockwise in the lower panels (northern hemisphere) and counterclockwise in the upper panels (southern hemisphere). Panels (a) and (b) from Kahru et al. (2007); panels (c) and (d) from Lévy & Klein (2004).

1370
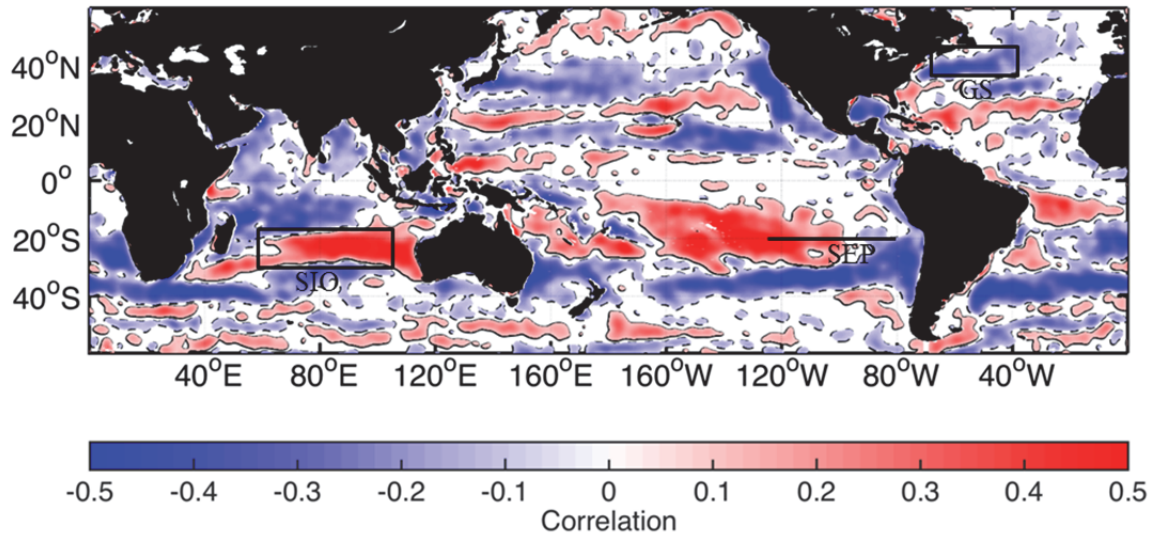
1371
1372 **Figure 9.** Map of the correlation between anomalies of sea level and chlorophyll. White areas
1373 correspond to correlations smaller than the estimated 95% significance level. Regions of
1374 significantly positive and negative cross correlations are enclosed by solid and dashed contours,
1375 respectively. Adapted from Gaube et al. (2014).

1376

a) eddy transfer

low nutrients

high nutrients

b) eddy and Ekman transfer

low nutrients

A   B   C
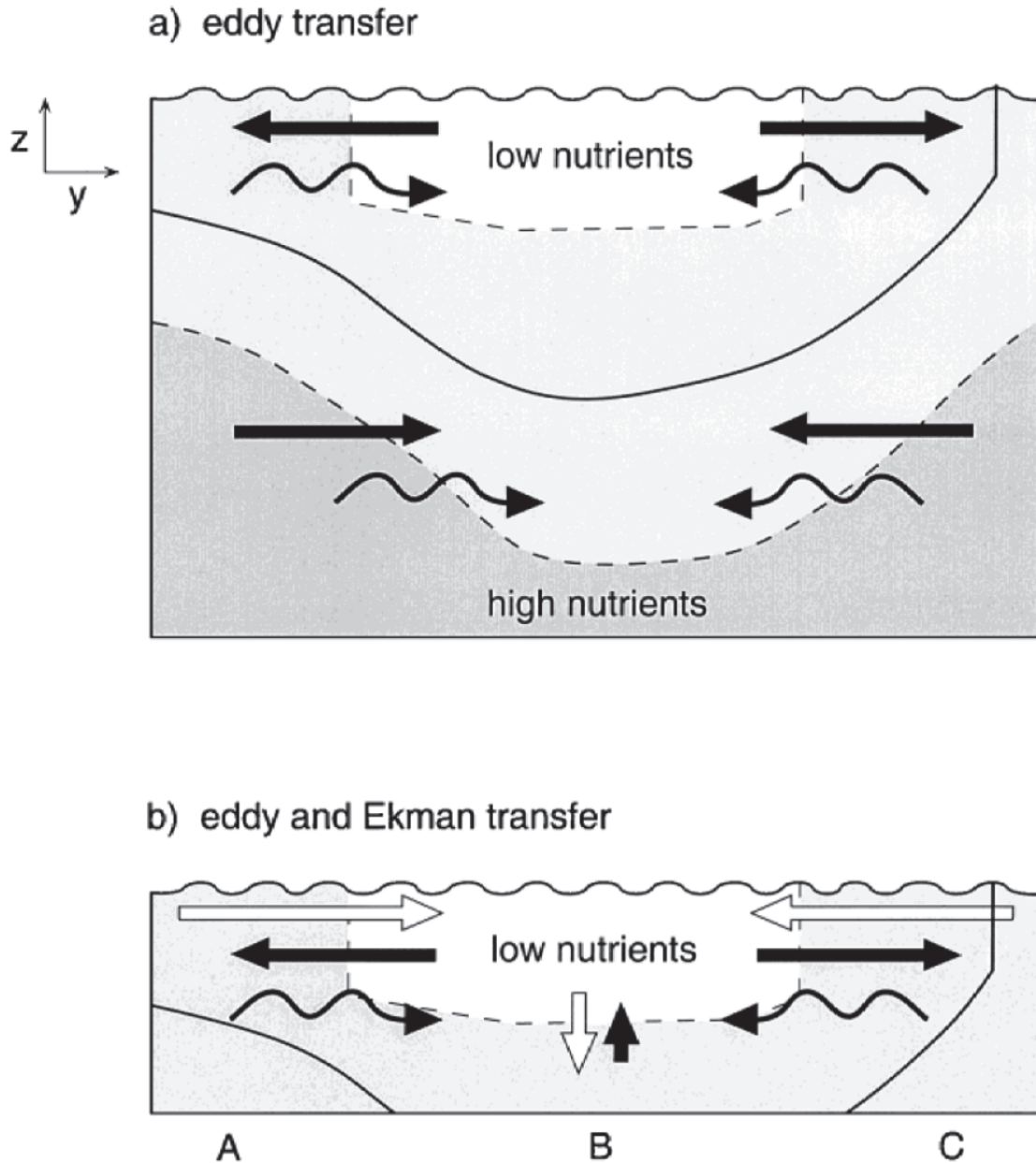
Figure 10. Schematic of the eddy-induced transfer of nutrients. SectionAC may be viewed as passing through a subtropical gyre or section AB as through the Southern Ocean. In (a), the eddy-induced advection (black straight arrows) and diffusion (curly arrows) oppose each other at the surface, but reinforce each other at depth. In (b), the Ekman advection (white arrow) is included. From Lee and Williams (2000).

40
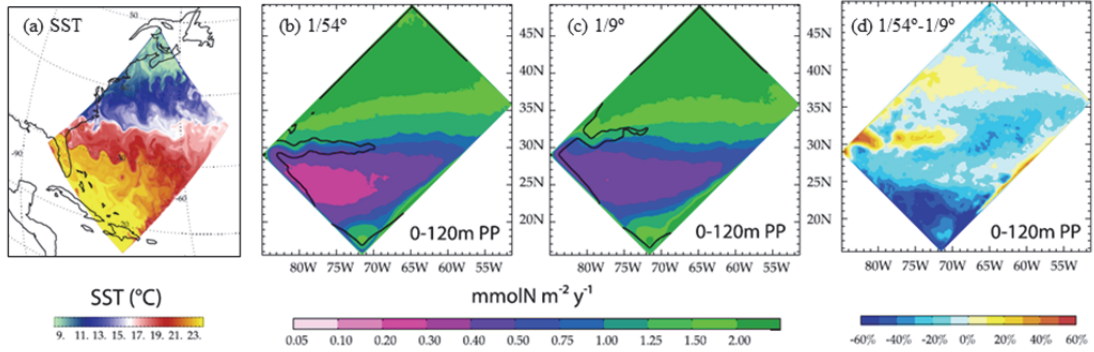
1387 **Figure 11.** (a) Sea surface temperature simulated in an idealized double-gyre system of the
1388 western North Atlantic. Panels (b) and (c) show five-year average depth-integrated (0-120m)
1389 primary production for 1/54º and 1/9º models after 50 years of integration; panel (d) shows their
1390 difference. Note the different map projection in panel (a) from Lévy and Martin (2013) versus
1391 panels (b-d) from Lévy et al. (2012b).
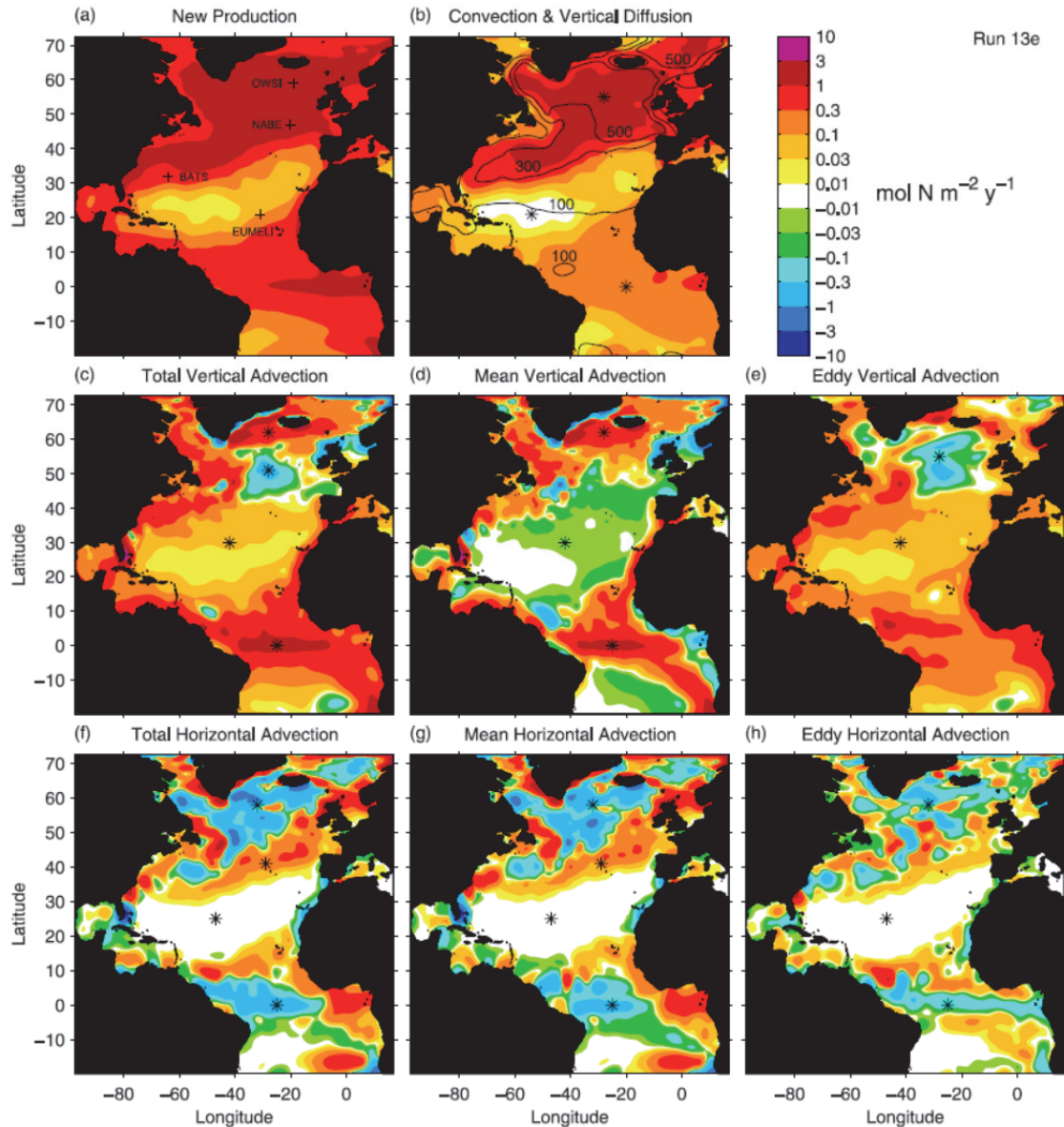
1395
1396 **Figure 12.** Five-year time-averaged new production (a) and nutrient supply terms (b-h),
1397 integrated over the euphotic zone. Advective fluxes in the vertical (middle row) and horizontal
1398 (lower row) have been separated into their mean and eddying components. All fields have been
1399 smoothed with a 24-point e-folding scale Gaussian filter. Asterisks indicate the main features of
1400 the solutions described in the text. Contours in Figure panel (b) indicate maximum wintertime
1401 mixed layer depths of 100, 300, and 500 m. Note that wintertime mixed layers inside the 500-m
1402 contour exceed that value by severalfold; additional contours are not shown for clarity of
1403 presentation. From McGillicuddy et al. (2003).
1404
1405

An Eddy-driven Nutrient Sink:
Mesoscale Restratification After Deep Convection

1406
1407
1408 **Figure 13.** Schematic of the eddy-driven processes that tend to restratify an area of deep
1409 convection in the open ocean. Inward flux near the surface and outward flux at depth imply a
1410 downward eddy-driven transport that removes nutrients from the euphotic zone. Note that the
1411 convective area does not represent an individual chimney but the larger region over which
1412 mesoscale and submesoscale convective events take place. From McGillicuddy et al. (2003).
1413
1414
1415
1416
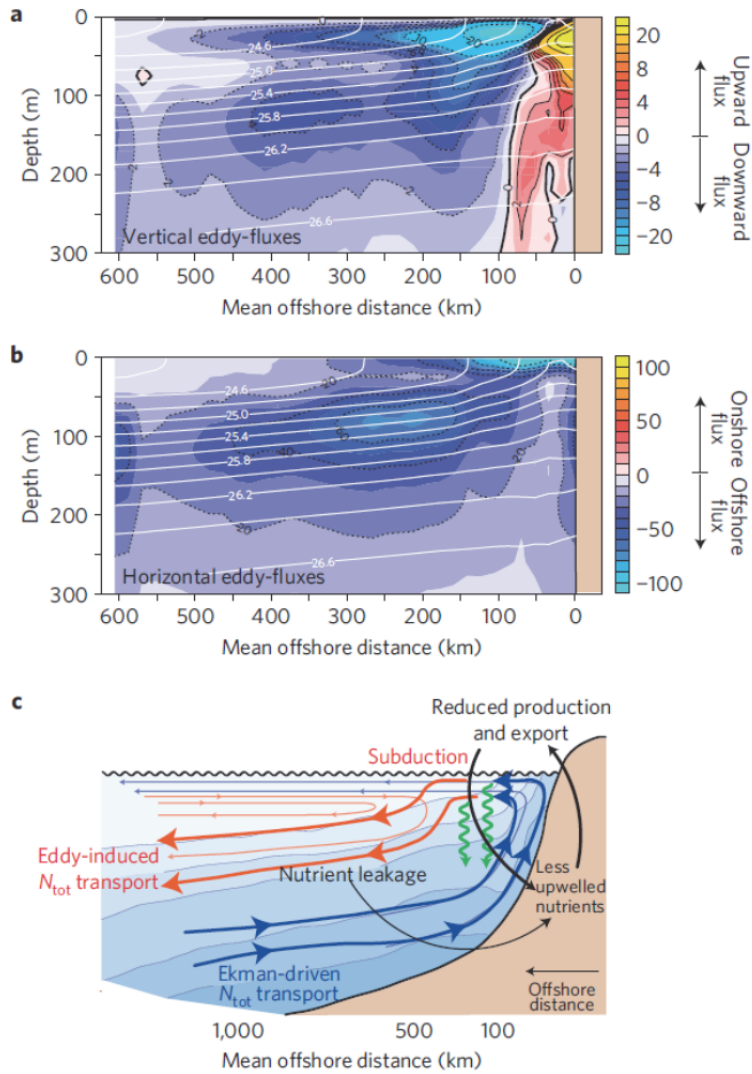
Figure 14. Cross-shore sections illustrating the role of eddies in inducing a lateral loss of total nitrogen from a model of the California Current system. Panels (a) and (b) depict vertical and horizontal fluxes of total nitrogen, respectively; units are nmol m^{-2} s^{-1}. White lines are potential density; black dashed lines indicate negative fluxes. Panel (c) depicts a conceptual diagram of the impact of mesoscale eddies on coastal circulation, nitrogen transport, and organic matter production and export. The thick lines indicate total nitrogen transports and the thin lines depict circulation pattern. Shown in blue are the Ekman-driven transports and circulations. The red arrows show the eddy-driven transports. Contour lines denote potential density and green arrows the vertical export of organic matter. From Gruber et al. (2011).
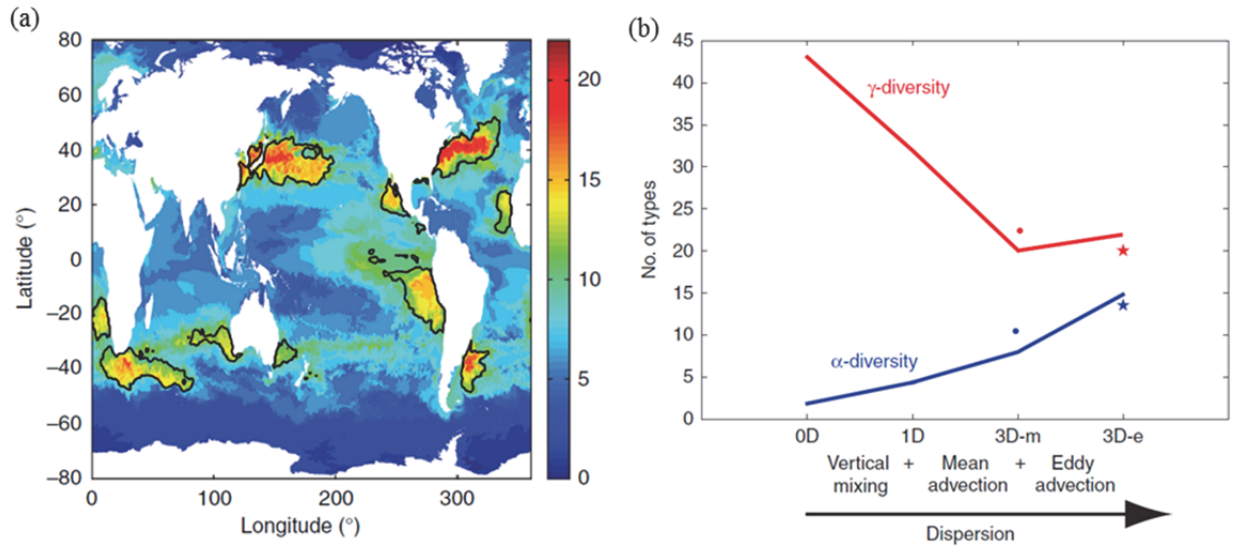
1429
1430 **Figure 15.** (a) Annual average diversity in the surface layer of the high-resolution (HR)
1431 configuration described in Clayton et al. (2013). Diversity (α) is defined as the total number of
1432 phytoplankton types with biomass greater than 0.001% of the total phytoplankton biomass. Black
1433 contour lines indicate phytoplankton diversity hotspots ($\alpha > 10.2$). (b) Trends in local diversity
1434 (α; 10-100 km scales) and regional diversity (γ; 1000 km scales) as a function of dispersion from
1435 the simulations described in Lévy et al. (2014). Experiments 0D, 1D, 3D-m, and 3D-e are
1436 ranked along the x-axis by increasing level of dispersion in the flow field. In the case with no
1437 dispersion (0D) each grid cell in the horizontal and vertical dimensions is treated independently.
1438 Vertical mixing is added in the 1D case, and advection by the mean velocity is added in the 3D-
1439 m case. The full eddy-resolving flow is accounted for in 3D-e. Results from the latter two
1440 experiments are marked with dots and stars, respectively.
1441
1442